PHASE-SHIFT MEASUREMENT ANALYSES OF TIME-LAPSE MULTICOMPONENT SEISMIC DATA OVER A MULTI-WELL HYDRAULIC STIMULATION, WATTENBERG FIELD, DENVER BASIN

by

Stephen W. Paskvich

A thesis submitted to the Faculty and the Board of Trustees of the Colorado School of Mines in partial fulfillment of the requirements for the degree of Master of Science (Geophysics).

Golden, Colorado

Date _____

Signed: _____
Stephen W. Paskvich

Signed: _____
Dr. Thomas L. Davis
Thesis Advisor

Golden, Colorado

Date _____

Signed: _____
Dr. Terence K. Young
Professor and Head
Department of Geophysics

ABSTRACT

Instantaneous phase calculations estimate phase differences in multicomponent seismic data between traces acquired pre- and post-stimulation of eleven horizontal wells in Wattenberg Field, Denver Basin. Estimated phase shifts illustrate the ability of multicomponent seismic to image the reservoir response associated with the interaction of stimulated, hydraulic fractures with natural fractures. Time-lapse shear-mode seismic showed the largest response with maximum phase differences of about 30 degrees. Converted-mode seismic provided shifts of about 20 degrees, and compressional-mode seismic gave shifts of about 15 degrees.

Instantaneous phase calculated for the crosscorrelation function of time-lapse traces windowed at the base of the reservoir provided the largest phase differences. Traveltime and phase differences both show that the western half of the reservoir where wells are more closely spaced responded more strongly to stimulation than the eastern half. Interpretation of simple 1D modeling, hydrocarbon production data, chemical tracer analysis, formation image logs, microseismic, and other seismic analysis suggests that measured phase differences correlate to regions of the reservoir where more fractures were opened during stimulation.

Phase shifts may measure attenuation and interference that results from the effects of hydraulic stimulation on propagating seismic energy and not just time or velocity like other measures. In unconventional reservoirs attenuation and interference may be more important mechanisms for change than velocity. Phase shifts measured in multicomponent seismic can provide relative information about fracture aperture, size, and orientation, and permanent reservoir monitoring could capture the dynamic response of reservoirs to widespread hydraulic stimulation as across Wattenberg Field. Multicomponent time-lapse monitoring, especially with phase-shift measurements, provides critical reservoir information unavailable through single mode seismic analysis or microseismic monitoring.

TABLE OF CONTENTS

LIST OF FIGURES

LIST OF TABLES

ACKNOWLEDGMENTS

This thesis has been made possible through countless blessings and graces, the patience and guidance of my committee, and the continuous support and encouragement of my wonderful parents, William and Christine. This thesis would not have been possible without the data and expertise provided by Anadarko Petroleum Corporation or the support of the Reservoir Characterization Project and its sponsors, to all of whom I would like to extend my sincere gratitude.

CHAPTER 1
INTRODUCTION

Hydraulic stimulation occurred in 11 wells drilled in the Wishbone section of the Niobrara and Codell Formations in Wattenberg Field, Colorado (see Figure 4.1). Anadarko Petroleum and the Reservoir Characterization Project at the Colorado School of Mines acquired time-lapse, multicomponent seismic data before and after stimulation, and White (2015) describes the data acquisition and processing. The total area covered by the seismic data is approximately 10.6 km^2. The baseline seismic was collected before hydraulic fracturing, and the monitor seismic after fracturing. Wattenberg Field is northeast of Denver, and a number of geologic formations including the Niobrara, the underlying Codell sandstone, and the shallower Hygiene and Terry sandstones produce oil, gas, and condensate. (Sonnenberg, 2013).

Recently, Burns et al. (2007); Fang et al. (2013a,b); Willis et al. (2006) proposed that differences in the phase of seismic wavelets extracted above and below reservoirs can be used to prospect for large fracture networks in 3D seismic. My research extends implementation of seismic phase to the time-lapse interpretation domain by approximating phase differences in multicomponent time-lapse data using the instantaneous phase measurement.

Instantaneous phase computed for crosscorrelated time-lapse traces approximates the difference in phase between the time-lapse traces. The approximation is reasonable provided that phase is constant or varies slowly along the traces or within a windowed segment of the traces. Such constraints were satisfied through the analysis of individual reflections. The calculations performed for this research showed that phase shifts, defined here as the difference in phase of a time-lapse reflection, exist between baseline and monitor surveys. Phase shifts indicate a change in the distribution of energy in time-lapse reflections. The measured time-lapse phase signal reveals clear patterns bounded by faults in the data, and

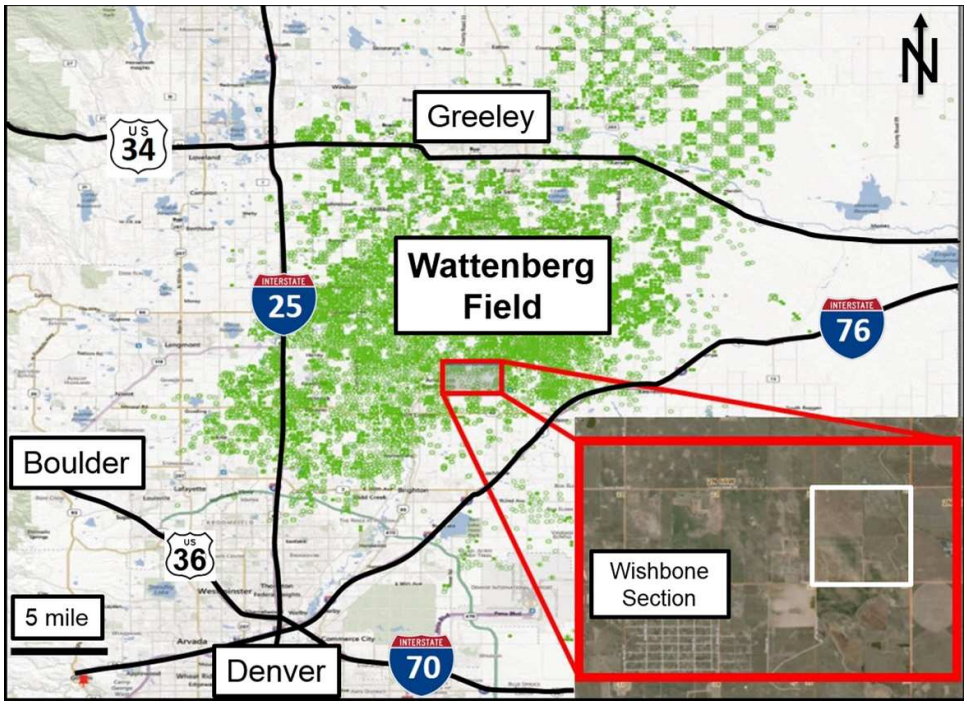

Figure 1.1: Map of Wattenberg Field showing the location of Wishbone section where 11 horizontal wells were stimulated in the Niobrara and Codell intervals. (Pitcher, 2015)

simple modeling considers possible causes for measured phase shifts. Interpretation of phase shifts in light of external data, such as microseismic and production data, suggests that the measured phase-shift response may result from interference and attenuation in the monitor seismic wavefield measured after well stimulation.

1.1 Geologic context and well completion summary

In the study area the Niobrara is approximately 90-m thick and consists of alternating chalk and marl layers with gradient contacts. Figure 1.2 shows a geologic column representative of the regional stratigraphy with hydrocarbon producing intervals marked. Since deposition, mechanical and chemical processes have fully compacted the Niobrara (Sonnenberg, 2013). Original porosities were as great as 50% but have been reduced to an average between 6% and 10% (Sonnenberg, 2013). Stimulation is necessary to economically produce hydrocarbons from the Niobrara and Codell intervals. The Niobrara is a self-sourcing reservoir, meaning that hydrocarbons that matured in place were trapped in place, filling the

in-situ porosity. Thus the Niobrara acts as source, seal, and reservoir.

The study area is heavily faulted, and faulting in the section may be part of a large, complex fault system observed regionally across Wattenberg Field. Fault geometry is an important factor for possible fluid and pressure migration and compartmentalization, particularly during hydraulic stimulation. Both fluid and pressure compartmentalization can affect the seismic wavefield, and White (2015) suggests that such is seen in these data based on interpretation of calculated acoustic impedance differences.

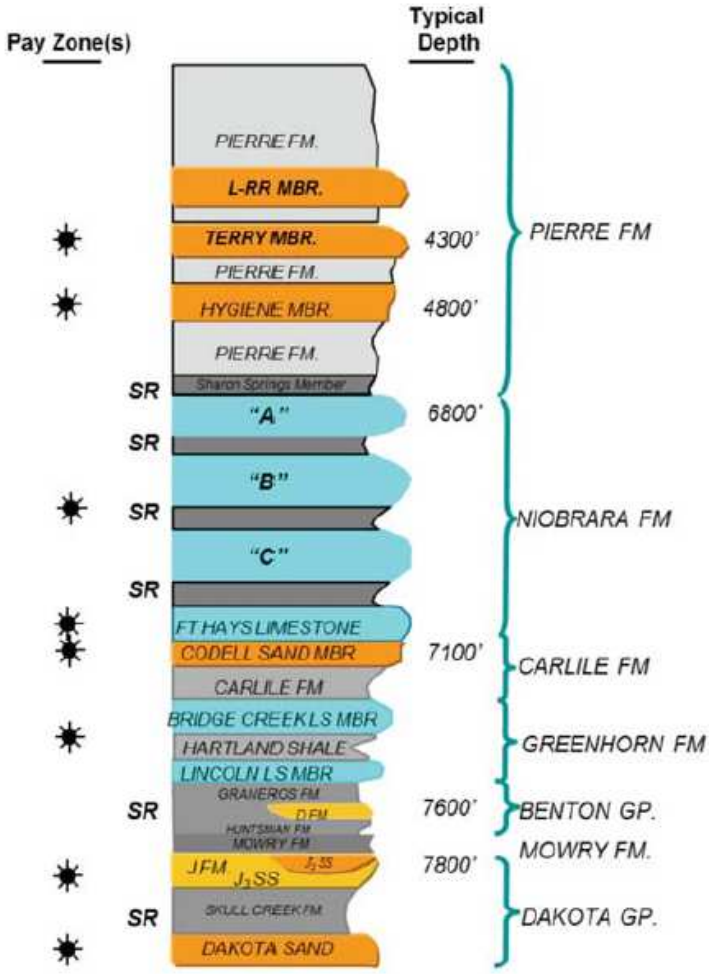

Figure 1.2: Regional stratigraphic column includes major geologic units present in Wattenberg Field. Black symbol to the left of the column denotes intervals that are currently producing. (Sonnenberg, 2013)

Seven of the 11 horizontal wells drilled in Wishbone section were completed in the Niobrara interval while four were completed in the Codell sandstone. Analysis by Dudley (2015) shows that wells are located in and outside of the targeted lithology along the length of each well, but Dudley (2015) suggests that lithology has negligible effect on well production. Spacing of wells and number of fracture stages per well were varied across the section along with pumping pressure, volume of fluid injected, size of proppant, and volume of proppant injected. Pitcher (2015) shows that little correlation exists between these completion variables and production at the individual well scale. Different methods of hydraulic fracture, including sliding sleeve, plug and perf, and zipper fracture were implemented in the section as well. The cross section shown in Figure 1.3 displays the general geological and spatial distribution of the 11 Wishbone wells.

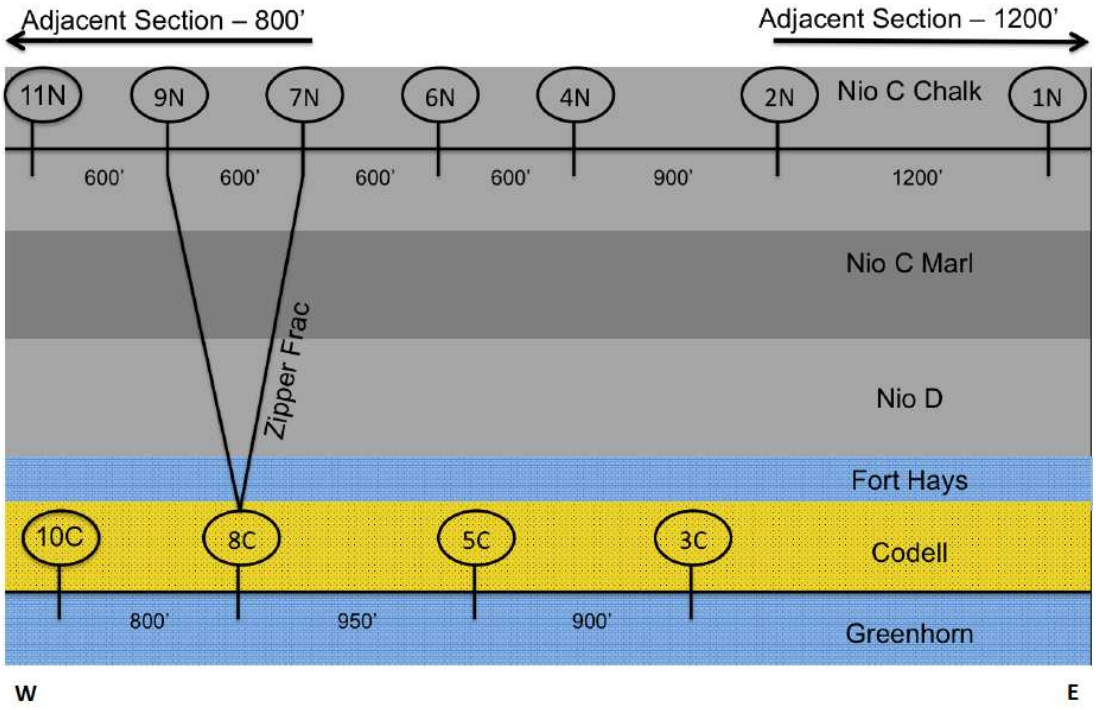

Figure 1.3: Simplified cross section of Wishbone section showing general well placement. (Pitcher, 2015)

CHAPTER 2

CALCULATION OF TRAVELTIME AND PHASE SHIFTS

Bishop and Nunns (1994) presented a method based on the complex seismic trace to calculate phase and traveltime shifts between different vintages of 2D seismic data. These scientists originally applied the method to estimate amplitude, traveltime, and phase angle corrections to reduce variations in amplitude, traveltime, and phase, respectively, between seismic data acquired at different times but that were not necessarily designed as time-lapse surveys. Implementation of this process towards those authors' original purposes has since become routine in time-lapse analysis workflows available commercially. Bishop and Nunns (1994) were interested in generating global corrections that involved many reflections to remove differences from their data. In contrast, my aim is to calculate and interpret traveltime and phase shifts only at particular reflections.

This thesis presents phase and traveltime shifts calculated for each pair of baseline/monitor traces in the time-lapse survey following the methodology laid out by Bishop and Nunns (1994). The crosscorrelation $R(t)$, where t is time lag, was computed between a baseline and monitor trace over a specified time window centered on a horizon picked on a reflection in the baseline volume of each mode (i.e., PP, PS, and SS). The window length used for crosscorrelation approximated the length, which varied for each mode of data, of the seismic wavelet in each baseline volume. Wavelet length windows are short enough to prevent unwanted reflections from affecting the crosscorrelation but long enough that the trace contains a full cycle. Choosing a window approximating the wavelet length ensures a reliable and locally meaningful crosscorrelation result since it captures the entire reflection of interest in both the baseline and monitor volumes even if they are not perfectly aligned.

In the PP data, the picked reflection used for calculation tied with the Bridge Creek reflector located near the base of the stimulated reservoir. In the PS and SS data, shifts

were measured at reflections near the base of the reservoir as well but do not necessarily tie to the Bridge Creek reflector. Table 2.1 gives the window length and location for each traveltime- (TS) and phase-shift (PHS) calculation. The shifts calculated at these reflections provided the largest shifts for each mode of data, and calculating shifts at a reflection at the base reservoir rather than across the entire reservoir interval ensures that all accumulated shifts are measured. Further, for the shear element of the converted-wave seismic to travel across the full reservoir interval, the mode conversion from compressional to shear must occur at or below the base reservoir. In light of this constraint, to meaningfully compare converted-wave shift results to results for the other modes, shifts must be calculated at similar locations in the compressional and shear modes.

Table 2.1: Parameters for phase- and traveltime-shift calculations

	Window length (ms)	TS calculation horizon	PHS calculation horizon
PP	80	Top Bridge Creek	Top Bridge Creek
PS	160	Deep 1 PS	Deep 2 PS
SS	190	Deep 1 SS	Deep 2 SS

The different calculation locations are related to the length of the seismic wavelet and bandwidth of each mode of data. Although the phase shifts in the compressional- and shear-mode data result from changes in the reservoir interval, since the shear-mode wavelet is longer, phase shifts manifest deeper in the seismic data. Figure 2.2 shows sections from each mode of data indicating the locations of the reflections used for calculations.

Complex seismic trace analysis provides the means for calculating traveltime and phase shifts. Here, the complex trace was composed of the real windowed crosscorrelation trace, which is a segment of the full seismic trace, and its imaginary conjugate. The Hilbert transform of the crosscorrelation trace generated the imaginary part of the complex trace, and envelope and instantaneous phase were calculated for the crosscorrelation function using the complex trace transforms described by (Taner et al., 1979) and outlined in the next section. The maximum value of the crosscorrelation envelope was found for each mode, and

the time $t = \tau$ at which the envelope peak occurred was the optimum time lag. This time lag is the traveltime shift between the baseline and monitor traces for the picked reflection. The value of instantaneous phase at $t = \tau$ is the phase rotation between the traces for the picked reflection. Figure 2.1 illustrates the process, and it is important to note that although a time shift is equivalent to a phase shift for single-frequency data, the analyzed field seismic data contain many frequencies, and there is a single combination of time and phase shift that matches the traces optimally (Bishop and Nunns, 1994).

2.1 Calculation of the complex seismic trace

Taner et al. (1979) notably described complex trace analysis for seismic signals, and since that time, the complex seismic trace has been used widely as the basis for seismic attribute analysis. Complex seismic trace analysis is a transform technique that provides trace amplitude and phase information while retaining local significance (Taner et al., 1979).

The complex seismic trace is composed of real and imaginary parts with the recorded seismic trace treated as the real part and the imaginary part, also known as the quadrature or conjugate trace, computed as the Hilbert transform of the real part.

For an arbitrary time series $x(t)$, its Hilbert transform, $y(t)$, is defined as

$$y(t) = \frac{1}{\pi} PV \int_{-\infty}^{\infty} \frac{x(t')}{t - t'} \mathrm{d}t', \tag{2.1}$$

where PV indicates the Cauchy principal value. The Hilbert transform gives a unique definition of the imaginary part such that $x(t)$ and $y(t)$ make up an analytic signal (Huang et al., 1998). The Hilbert transform is a convolutional operation and can simply be considered as a filter that shifts phases of all frequencies contained within the signal by a magnitude of 90 degrees (Purves, 2014). The Hilbert transform may be applied alternatively by 1) Fourier transforming a real seismic trace; 2) multiplying all negative frequencies by i, that is $\sqrt{-1}$, and all positive frequencies by $-i$; and 3) inverse Fourier transforming the modified trace. Multiplying all frequencies of the Fourier transformed trace, which is made up of complex numbers, by either i or $-i$ is equivalent to a phase rotation of 90 degrees.

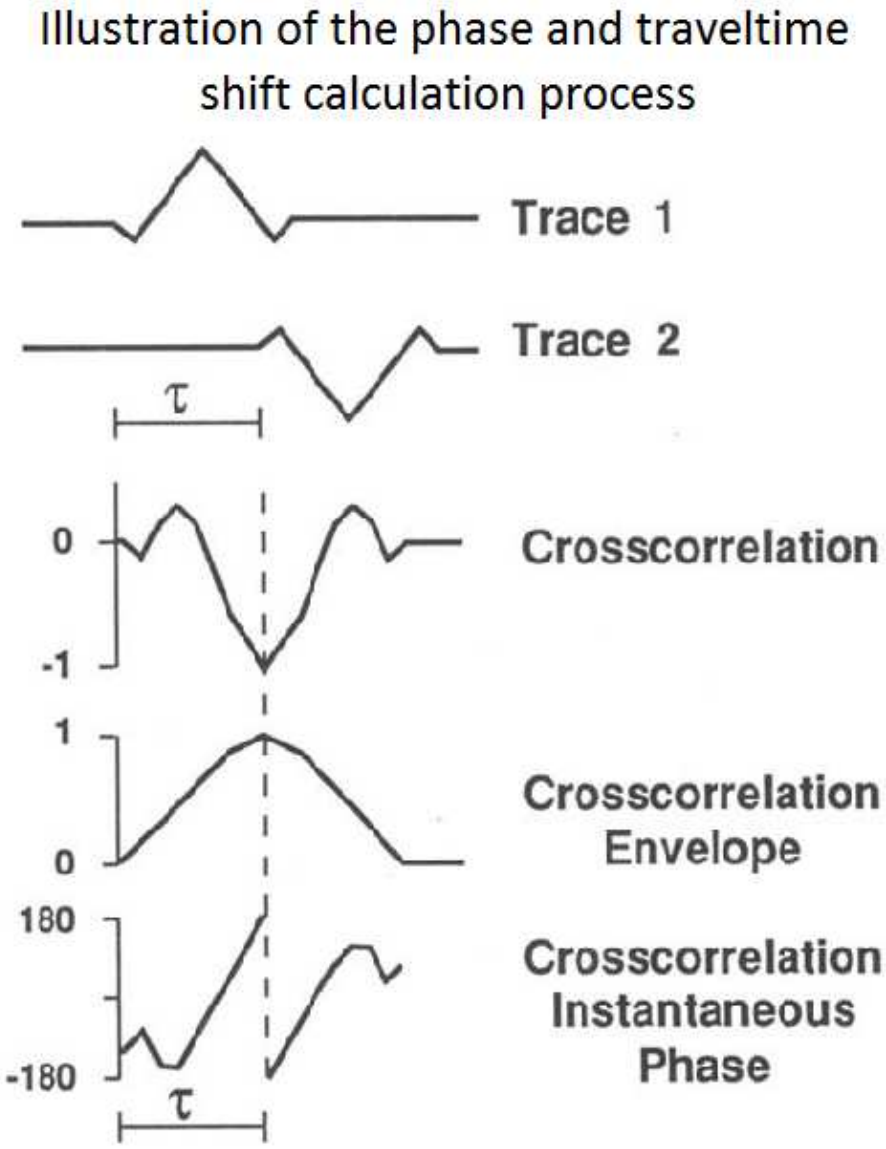

Figure 2.1: Illustration of the phase and traveltime-shift calculation methodology. Trace 2 is a 180-degree phase-rotated version of trace 1 that is also shifted in time. The traces are crosscorrelated, and the envelope of the crosscorrelation trace is generated. The time at which the peak envelope value occurs gives the traveltime shift to correct trace 2 to trace 1 in time. The instantaneous phase of the crosscorrelation trace at this same time approximates the phase shift between the traces. All calculated phase shifts range between -180 and 180 degrees because the instantaneous phase is calculated from the inverse tangent function. (Bishop and Nunns, 1994)

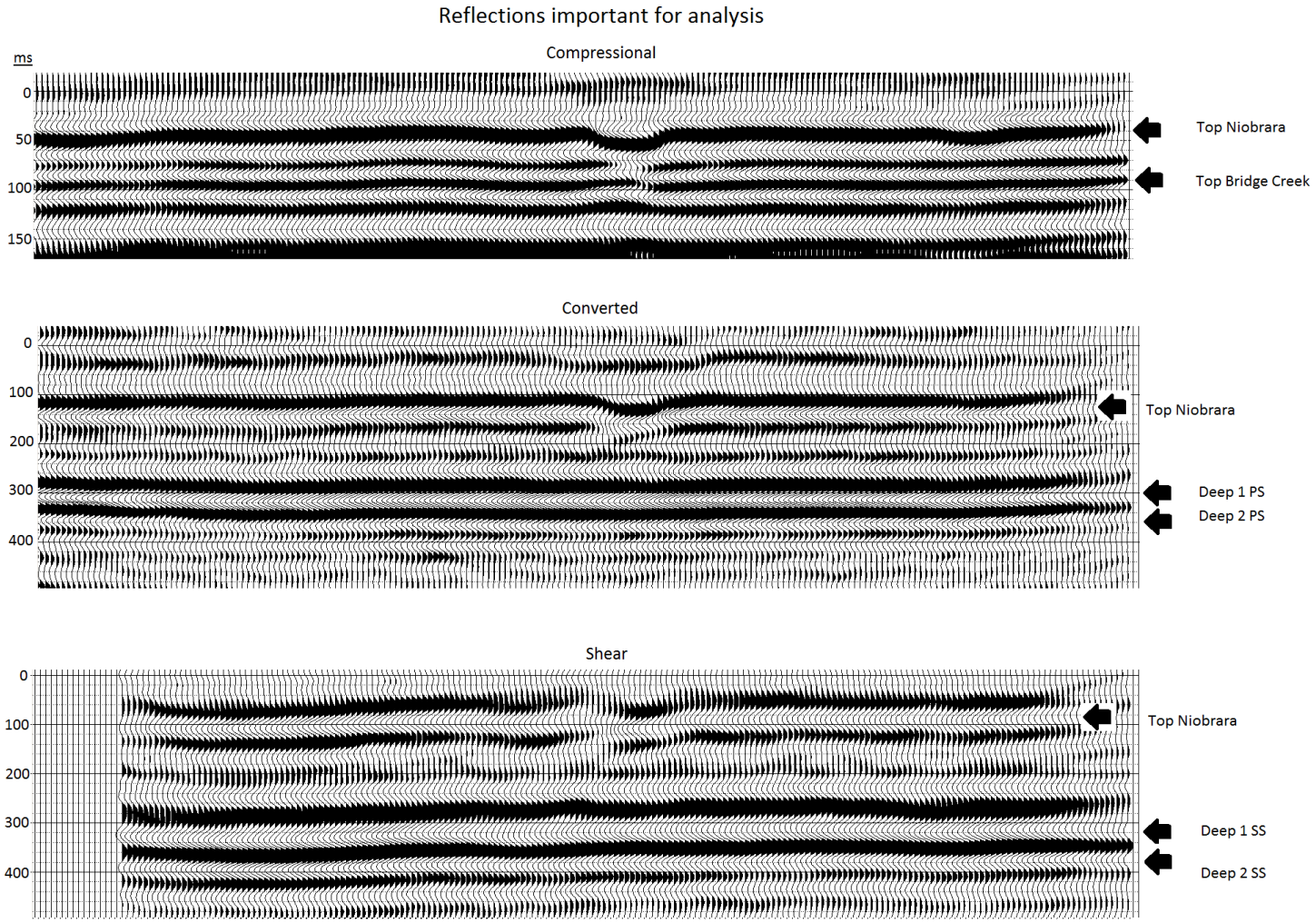

Figure 2.2: Sections for each mode of seismic data highlighting important analysis reflections including the Top Niobrara reflection and the deeper reflections used for calculating traveltime and phase shifts. Time scales are relative, and the Top Niobrara reflection is confidently registered while the base reservoir reflections approximate the same reflectors.

With this definition, if the real seismic trace is represented as the function $x(t)$, then the imaginary component $y(t)$ is determined from the Hilbert transformation of $x(t)$. The components $x(t)$ and $y(t)$ together construct an analytic signal - here, the complex seismic trace. It follows that the complex seismic trace may be expressed as

$$c(t) = x(t) + iy(t). \tag{2.2}$$

The complex seismic trace may be expressed in polar form as

$$A(t)\exp^{i\theta(t)} = c(t) = x(t) + iy(t), \tag{2.3}$$

where $A(t)$ is envelope and $\theta(t)$ is instantaneous phase. Coordinate transformation of the complex number representing the complex trace from Cartesian to polar form allows the determination of the envelope and instantaneous phase quantities. Recalling that $y(t)$ is defined as the Hilbert transform of $x(t)$, then

$$A(t) = \sqrt{x(t)^2 + y(t)^2}, \tag{2.4}$$

and

$$\theta(t) = \tan^{-1}\left(\frac{y(t)}{x(t)}\right). \tag{2.5}$$

2.2 Discussion of instantaneous measurements for time-lapse characterization

The trace attributes of amplitude, traveltime, and phase, which interact complexly, must be separated for their meaningful interpretation. One important question is whether instantaneous phase, which is a point value at a single trace sample, adequately estimates the phase difference between reflection events and portions of the seismic trace that extend over multiple samples. This consideration begins with a description of the complex seismic trace components, envelope and instantaneous phase, followed by how these components separate the trace variables, and finishes with some discussion of phase, including a demonstration that in a general case instantaneous phase values characterize well phase differences between time-lapse reflections.

Trace amplitude at a particular sample along the seismic trace will change if the phase of the trace is rotated. The amplitude at that sample will reach a maximum for a single, specific phase rotation. This maximum amplitude that a seismic trace can have at a particular time is called envelope (see Figure 2.3). The phase rotation required to attain that maximum amplitude value is called the instantaneous phase, and the envelope and instantaneous phase quantities can be found by incrementally rotating the phase of a seismic trace. Alternatively, computation of the complex seismic trace provides these quantities through a mathematical transformation. Much as the Fourier equations are a convenient mathematical tool to extract frequency-dependent information from the recorded seismic trace, the complex seismic trace is a mathematical tool that can be used to extract amplitude and phase information along a recorded seismic trace.

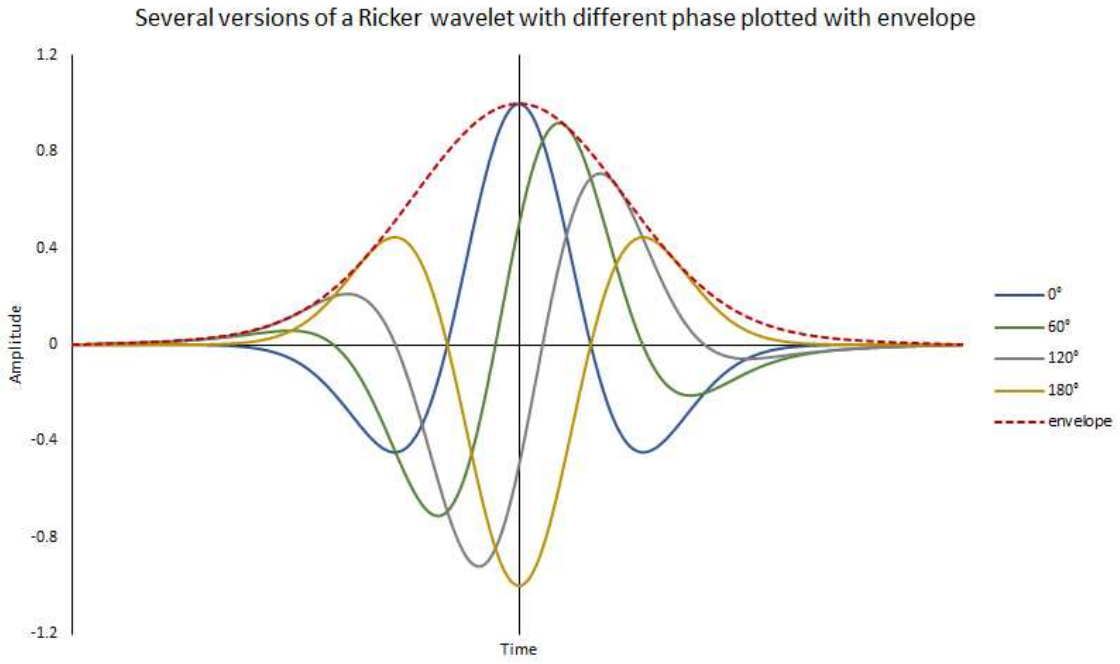

Figure 2.3: Several wavelets with different phase and equivalent envelope. Envelope shown by the dashed red line. Instantaneous phase calculated for the 60 degree wavelet at the time axis origin, for example, results in an instantaneous phase value of 60 degrees. With this rotation the amplitude at the time origin becomes equivalent to the envelope value there.

An advantage of complex trace analysis is that it allows the interpreter to consider envelope rather than raw trace amplitude. Envelope is independent of phase and is often referred to as "reflection strength" (Sheriff et al., 1977). Reflections from major geologic interfaces, such as shale/limestone contacts and unconformities typically have large reflection strength (Taner et al., 1979). Maximum envelope values occur at points other than amplitude maxima or minima along the recorded seismic trace when a reflection is a composite of several interfering reflections or when the seismic data have not been adequately zero-phased during processing. Since amplitude, unlike envelope, of the seismic trace is dependent on phase, amplitude peaks or troughs may not be simply associated with geologic interfaces. Consequentially, envelope can be a more reliable indicator of major geologic boundaries than recorded trace amplitude peaks or troughs.

Extending this concept to the present work, a crosscorrelation trace generated from recorded seismic traces is a function of time-dependent amplitude and time-dependent phase just as are the input recorded seismic traces, and the peak crosscorrelation does not necessarily correspond to the peak envelope. Shifts determined from the maximum amplitude of a crosscorrelation trace represent a weighted amplitude, that is, a correlation strength weighted by phase. Trace differences from such a composite cannot be interpreted clearly. Rather, the maximum correlation strength, given by the maximum envelope, which represents optimal trace alignment, must be located and separated from the phase information contained within the crosscorrelation trace. Correlation strength and instantaneous phase calculated from the complex seismic trace separate the amplitude and phase information, which can be manipulated and interpreted independently, contained in the crosscorrelation trace.

Although raw trace amplitude peaks do not necessarily represent the exact location of geologic interfaces, reflections, which are here considered as a collection of samples preceding and following a trace amplitude peak or trough, are often used to represent the geophysical manifestation, which includes more than location information, of a geologic interface. The

complex seismic trace provides a way to inspect time-lapse reflection strength, traveltime, and phase distinctly. Although reflection strength is not considered here directly but its counterpart, correlation strength, which provides the optimal alignment of reflections, is used to derive traveltime information while instantaneous phase is used to extract information about the phase of reflections. Both correlation strength and instantaneous phase correspond to a single sample, only a piece of a reflection. This locality is an advantage, since calculations show (Figure 2.4) that instantaneous measurements reasonably describe whole reflections, as have been defined here. Precise examination of single reflections is possible, and instantaneous phase values, specifically, relate information about local trace phase.

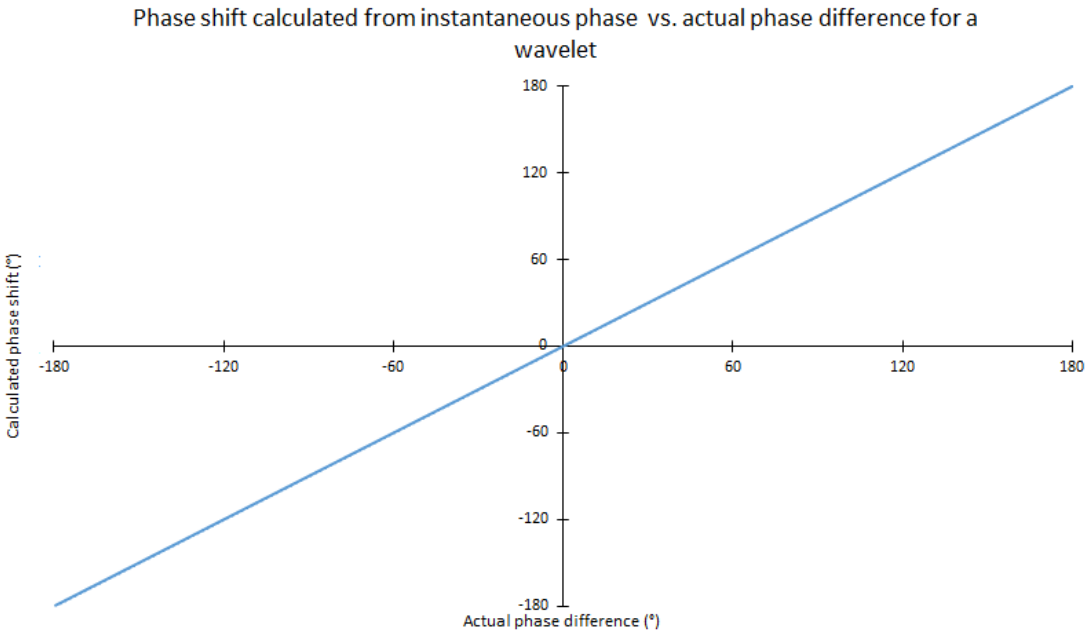

Figure 2.4: Phase-shift calculation accurately estimates the phase difference between wavelets. Calculated instantaneous phase value (phase shift) for the crosscorrelation of two wavelets with different phase plotted against the actual phase difference between the wavelets. The phase difference between the wavelets is calculated even though the wavelets have length while the instantaneous phase is computed at a single point along that length.

Instantaneous phase estimates the local phase difference. It is the phase rotation, the change in the distribution of signal energy, necessary to maximize the correlation strength of the crosscorrelation trace. Thus it estimates the phase rotation that matches the monitor

to baseline trace, that is, the phase difference between the baseline and monitor traces. The instantaneous phase provides an accurate difference in the case that the calculation window completely contains the time-lapse reflection of interest and that phase is constant or varies slowly along a reflection. Both criteria are met in the data considered in this thesis.

CHAPTER 3

MODELING

This simple convolutional model allows alteration of synthetic seismic reflections, and application of the method of Bishop and Nunns (1994) generates phase and traveltime shifts between simulated baseline and monitor synthetic reflections. In the same way that phase and traveltime shifts were calculated in the field data for many pairs of traces, synthetic shifts are generated for a single pairs of traces. This model investigates the sensitivity of traveltime and phase shifts as well as what they may physically indicate.

Three specific causes for phase shifts are considered as possibilities: source wavelet phase, attenuation, and interference. Different source wavelet phase would cause the signal phase to be systematically and initially different, while attenuation could continuously perturb wavelet phase during propagation, possibly causing local variations of signal phase. Simply changing input wavelet phase simulates both phenomena. Interference causes nearby reflections to interfere constructively or destructively, and changes in interference, therefore, effectively cause reflected energy to be distributed differently, which alters signal phase. Blending multiple synthetic reflections simulates interference in the model.

3.1 Methodology

A reflection constructed from the convolution of a zero-phase, 25-Hz Ricker wavelet (following Costain and Çoruh (2004)) with a reflection series representing a two-layer earth generated a synthetic baseline trace. This generates only a pseudo-reflection since the model does not simulate two-way propagation. Conceptually the seismic source is located at the ground surface while the receiver is located at the bottom of the geologic column. Test traces, representing monitor traces in the real seismic, resulted from a similar construction with different input parameters for wavelet phase, frequency, amplitude, and timing. Phase was varied between ± 20 degrees, reflection timing was varied separately by ± 10 ms, and

frequency and amplitude parameters are not reported, since they induced no measurable phase or time shift.

Another set of test traces represented a modification of the control two-layer earth with the insertion of a thin, third layer within the first layer. Reflectivity of the third layer varied between values of ± 0.015, and two scenarios with different distance (5 ms or 20 ms) between the third layer and initial interface tested interference effects. The inserted layer very generally simulates the introduction of fluid-filled fractures to a finite volume completely contained within a single geologic unit, and Figure 3.1 provides a schematic that illustrates the model concept. The method of Bishop and Nunns (1994) calculates the phase and traveltime shift between each test trace and the baseline trace.

3.2 Results of modeling

Table 3.1 reports the calculated values of phase and time shift for varying input wavelet phase. The phase shift was reproduced accurately while the time-shift measurement showed no sensitivity to changing wavelet phase. Error in the phase measurement increased as the magnitude of phase shift increased.

Table 3.2 reports the results for the second test in which phase and time shifts were calculated between the control and test traces for constant phase and varied reflection traveltime. Phase showed no response to altered reflection timing, and the applied time shifts were calculated exactly. These results show that the calculation itself is accurate and, in this synthetic case, that variations in phase have little effect on the measurement of traveltime shifts and that variations in traveltime have little effect on phase-shift measurements.

The results of the thin layer test show a visible change in the reflection as can be seen in (Figure 3.2), and Figure 3.3 plots measured phase shifts for the two different scenarios of the thin layer test. The two tests provide trends with different slope sign and magnitude. The phase-shift measurement responded differently based on the proximity and magnitude of the synthetic reflections (i.e., how the reflections interfered). As the proximity and magnitude of the synthetic reflections varied, the reflections interfered differently, which impacted the

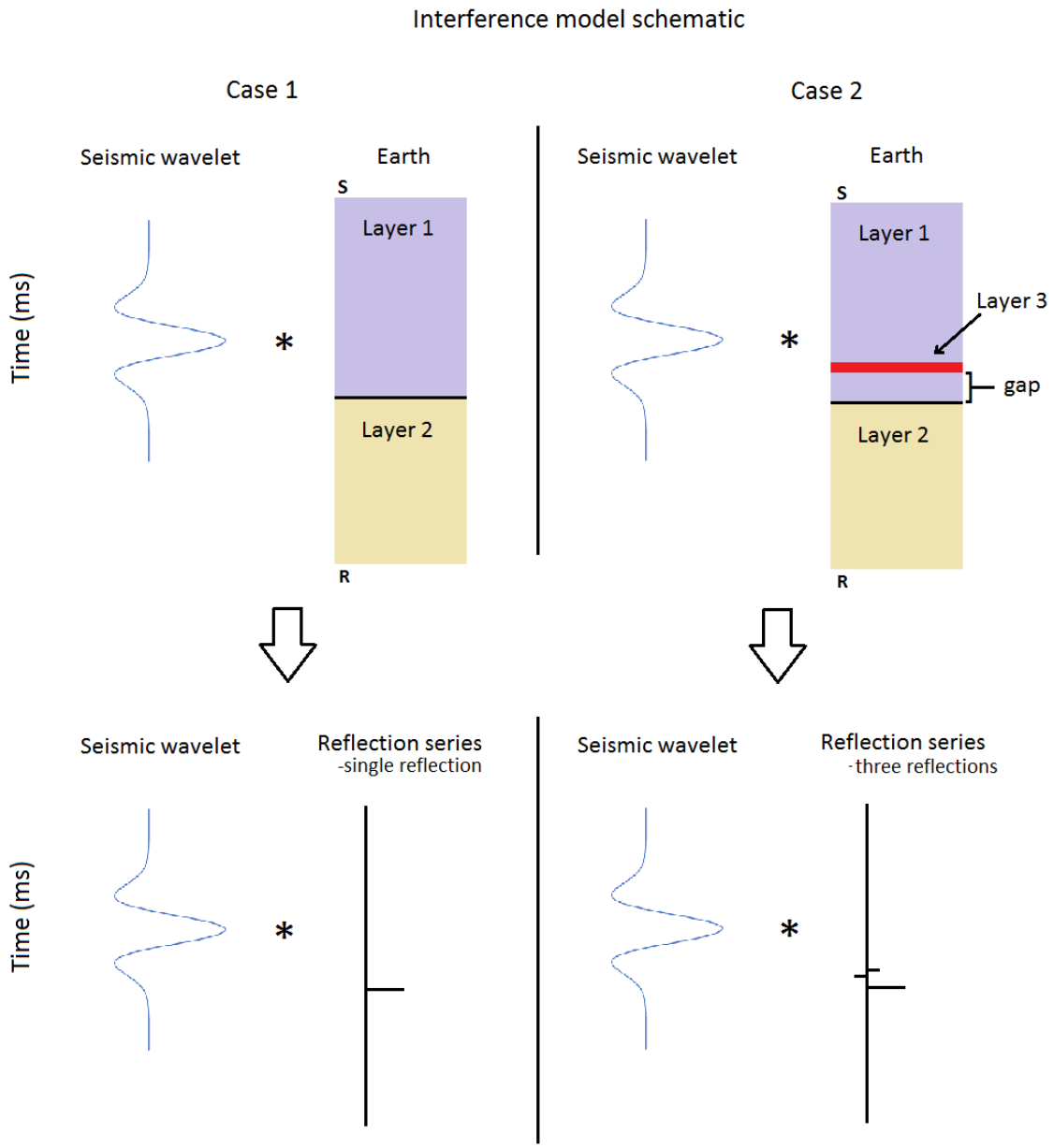

Figure 3.1: Illustration of the model designed to test the phase and time response to interference. The lower half of the figure shows the same as the upper half but with the conceptual geologic sections shown as reflectivity series. In Case 2, the embedded Layer 3 is designed to simulate a thin, fractured interval composed of the same material as the surrounding Layer 1. The seismic source is located at the top of Layer 1 and the receiver is located at the base of Layer 2.

Table 3.1: Results of phase- and time-shift measurements for an applied shift of wavelet phase

Applied phase shift (degrees)	Calculated phase shift (degrees)	Calculated time lag (ms)
-20	-20.2	0
-15	-15.2	0
-10	-10.1	0
-5	-5.1	0
-0	0	0
5	5.1	0
10	10.1	0
15	15.2	0
20	20.2	0

response of the phase measurement.

Changing the window length and location influenced calculations greatly. Depending on window size and alignment, traveltime-shift values could vary by up to 2 ms, and phase shifts could vary by up to 10 degrees. Using different lengths of windows and locations also showed that traveltime and phase shifts were most accurately measured in different places for more complex signals containing additional reflections compared to those illustrated in Figure 3.2.

3.3 Interpretation of modeling results

First, modeling again showed that the methodology of Bishop and Nunns (1994) provides accurate phase and traveltime-shift measures. The measurements were largely independent of one another, and errors from modeling fall below the resolution of measurement in the field data, based on comparison to error analysis in the field data. For more complicated signals involving more reflections, the calculation is less accurate in distinguishing between traveltime and phase shifts, however. Modeling further shows that while phase- and traveltime-shift measures are insensitive to changes in frequency or amplitude of the input wavelet, they can indicate both changes in wavelet phase as well as changes in interference patterns between time-lapse signals.

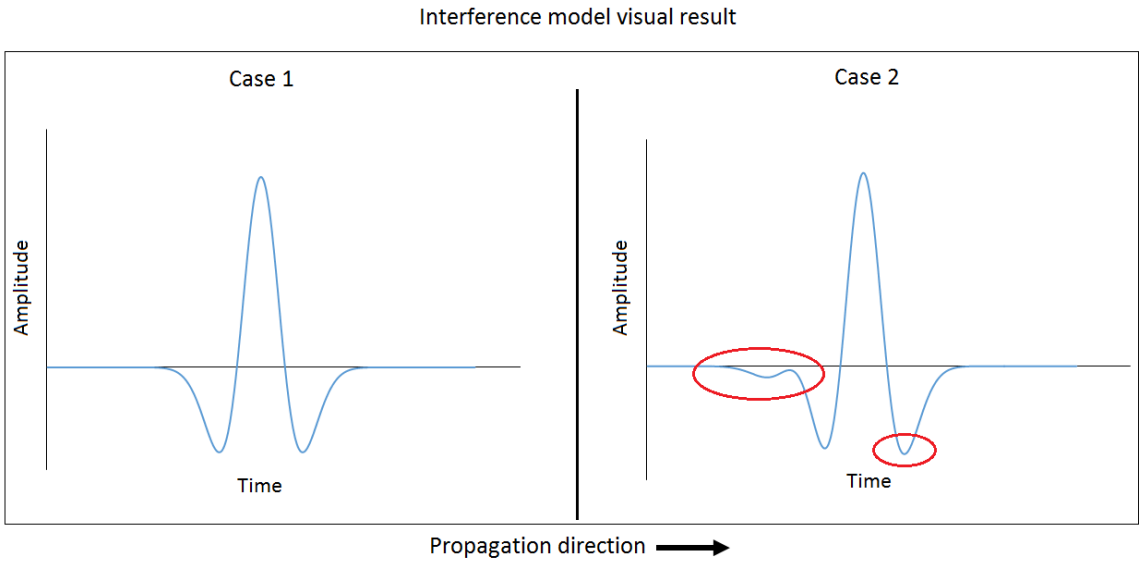

Figure 3.2: Comparison of the baseline synthetic reflection and the reflection generated with an inserted layer. The reflection on the left is the baseline reflection. The reflection on the right is a test reflection generated with an inserted third layer. The leading side lobe of the test reflection as well its tail differ from the baseline reflection.

Modeling provides no expectation of sign for phase shifts measured in the field data and suggests that window length and location are imperative for making accurate shift measurements, since traveltime and phase shifts were best measured from different windows in these tests. Traveltime shifts were best measured around the main lobe of the reflection of interest while phase shifts were measured most clearly in windows centered around the trailing lobe of the reflection of interest. The modeling supports that measuring traveltime and phase shifts in different windows, as was done in the converted- and shear-mode field data, is a reasonable practice. This is explained not only by the difference in velocity between each mode but by the difference in bandwidth per mode which results seismic wavelets of different length. In the compressional and converted data, the tail of the reflection is nearer to the main lobe of the reflection relative to the similar measure in the shear data, since the shear data contains a longer wavelet. Thus, for example, traveltime and phase shifts occur closer together in the converted-mode seismic than in the shear-mode seismic.

Table 3.2: Results of phase- and time-shift measurements for altered reflection timing

True time lag (ms)	Calculated phase shift (degrees)	Calculated time lag (ms)
-10	0	-10
-8	0	-8
-6	0	-6
-4	0	-4
-2	0	-2
0	0	0
2	0	2
4	0	4
6	0	6
8	0	8
10	0	10

Integrating these results into the larger study and considering one of the suggested possibilities responsible for differences in the phase of the time-lapse data, a difference in source wavelet causing phase shifts is unlikely, since a systematic phase shift would be measured throughout the data. No systematic shift is discernible in any of the data. Considering the care taken to repeat seismic acquisition precisely makes a difference in source wavelet an unlikely explanation for phase shifts measured in the field data as well.

The possible impacts of attenuation and interference are more difficult to distinguish. Frequency dependent attenuation, a reduction in amplitude of specific frequencies in the monitor survey compared to the baseline survey, was measured in the reservoir, and attenuation is known to alter phase. Interference also certainly occurs, since the seismic trace is inherently composed of interfering seismic reflections. The extent to which interference patterns differ between the baseline and monitor field traces is unclear, though. That attenuation may even be a result of interference further complicates assigning phase shifts to one or the other phenomenon (Lee et al., 2002), and phase shifts measured in field data certainly result from a combination of both.

It may be expected that where phase shifts are measured greater differences in attenuation and/or interference in the seismic wavefield occur between baseline and monitor surveys. The

mechanisms for either effect remains unknown, and external data are needed to draw any conclusions. Both attenuation and interference are considered as possible sources for phase shifts during interpretation.

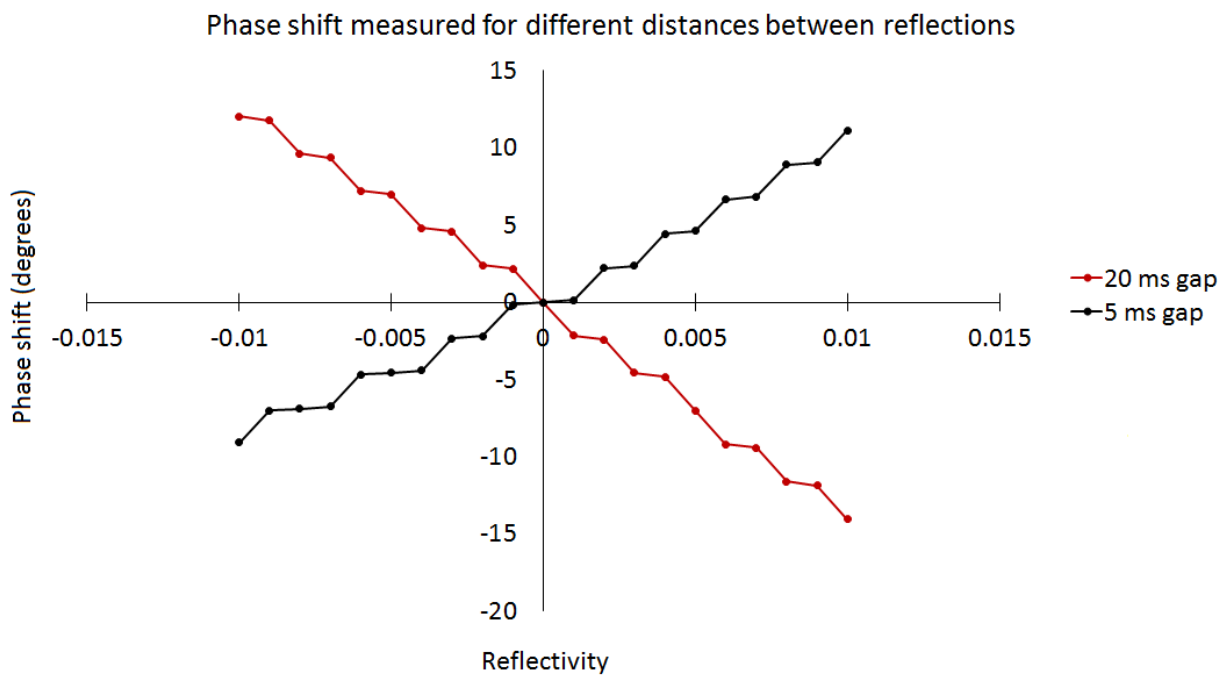

Figure 3.3: Plot showing phase shift as a function of reflectivity for two different thin layer tests. One test was performed with a 20 ms distance between the base of Layer 3 and the top of the Layer 2. The other test was performed with a 5 ms distance between the base of Layer 3 and the top of Layer 2.

CHAPTER 4

RESULTS OF PHASE- AND TRAVELTIME-SHIFT CALCULATIONS

Phase and traveltime shifts show varied results among the different modes of seismic data. At the end of the chapter shifts are presented as maps of values colored by magnitude. Faults are shown, and the timeline next to each figure shows which wells were stimulated during seismic acquisition. Colored well toes correlate to timeline colors. Wells truncated by squares indicate wells that continue off of the map.

Traveltime shifts were not observed in the compressional mode of the data, and only phase shifts are reported for this mode. Converted- and shear-mode data showed both traveltime and phase shifts. In each mode shifts were calculated at reflections near the reservoir base. For all data the measurement at the base reservoir represents the accumulated phase shift for the entire volume of data above the reflection. It also includes shifts accrued along both the down-going and up-going ray paths of the recorded seismic energy.

These data were cross-equalized, and after cross-equalization these data were highly repeatable. After cross-equalization shifts observed at the base reservoir, especially in high fold regions of the survey, could be safely interpreted as real changes recorded in the seismic caused by physical changes in the subsurface. The only significant changes occurring in the subsurface between baseline and monitor surveys took place in the reservoir interval, and all observed shifts can be attributed to effects of the hydraulic stimulation.

In maps shift values indicate the change in phase or traveltime necessary to match the monitor seismic to the baseline seismic. Both positive and negative phase shifts represent a change in the seismic data. A negative traveltime shift shows that traveltime was greater in the monitor seismic than the baseline seismic, while a positive traveltime shift shows that traveltime was less in the monitor seismic than the baseline seismic. A negative traveltime shift indicates that the seismic was slower after stimulation.

4.1 Compressional-wave phase shifts

Figure 4.1 shows phase shifts measured around the base reservoir reflection in an 80-ms window, which approximates of the length of the seismic wavelet in the PP data. Black, dashed lines represent faults, which are modified from White (2015). Shifts range between -15 degrees and 15 degrees, and the most prominent shifts lie around the Wishbone wells, particularly those in the western half of the section. In high-fold areas of the map, shifts are near zero or positive. There is no expectation as to whether positive or negative phase shifts should be observed, and either could represent real signal. Shifts near the edges of the survey are considered more cautiously since these areas of the survey are lower fold.

Some shifts lie to the west of Wishbone section and coincide with the locations of several nearby wells. The largest magnitude phase response covers the northwest of Wishbone section where some of the most closely spaced wells drilled in Wishbone lie in close proximity to three large faults. Subtle phase shifts surround wells to the east and west of Wishbone section as well, but shifts are not observed around all exterior wells imaged by the seismic.

Phase shifts appear to surround and truncate near faults. Around Wishbone wells, faults bound and compartmentalize the phase shift response. Phase shifts across the survey follow fault geometries as well. However, phase shifts do not appear around all faults. Near the edges of the survey most shifts are negative and correlate to fault locations. Negative or zero-valued shifts exist in areas where stimulations have recently taken place.

4.2 Converted-wave phase shifts

Figure 4.2 and Figure 4.3 show phase shifts for the fast and slow modes of the converted-wave data, respectively. The phase measurement made for the fast polarization showed a stronger response than that for the slow polarization. In both polarizations shifts range between -20 and 20 degrees. The fast polarization phase measurements show a greater response in the west of Wishbone than in the east, similar to the compressional data. In the east of Wishbone phase shifts surround the heel and toe of several wells, but the areas around

the intermediate length of the wells shows little response. Interestingly, in both polarizations the largest phase response correlates with wells located to the west of Wishbone section. Shifts do not exist around all surrounding wells, though. Faults again compartmentalize the phase shifts.

The largest shifts in the fast converted-wave data are west of Wishbone. The wells in this part of the survey were stimulated during a similar time period to the acquisition of the monitor seismic survey. In other parts of the survey, phase shift magnitude decreases with earlier stimulation dates. Stimulations after completion of monitor seismic acquisition show no phase response. Subtle phase shifts appear around wells stimulated much earlier (2 years) before time-lapse acquisition, but these shifts may not be related to the wells they surround. The lone well in the south east of the survey that shows positive shifts lies in an area where seismic was not acquired and was interpolated for this survey. Thus the observed positive shifts may not be reliable measures of the subsurface. In the southeast, negative shifts surround the radial well pattern, but the shifts appear along faults or fault tips. Phase shifts extend from recently stimulated areas along faults, and it may be that phase shifts around these wells are caused by physical changes in the subsurface extending from stimulated areas into other parts of the subsurface. The distribution of phase shifts across the reservoir appears to be highly related to fault geometries.

Fewer shifts occur in the PS2 data, but similar to the PS1 phase shifts, the largest appear west of Wishbone. Shifts also relate to fault geometries. The difference in response between the polarizations suggests an azimuthally anisotropic response. Conceivably, the fast converted-wave, which is polarized at approximately N70W, encounters and images a larger change in the reservoir. However, the difference in response depends on the medium symmetry and rotation of the polarizations. A different rotation of the fast and slow converted-wave data during processing could change the difference in response.

Fewer shifts around the edges of the survey appear in the converted data than in the compressional data. Particularly in the PS1 data, more distinct shifts appear than in the

compressional data. The large shifts in the west in both polarizations are reliable measures and not simply related to edge effects, since no shifts occur at overlying reflections for either polarization. These large shifts appear only below the stimulated reservoir

4.3 Converted-wave traveltime shifts

Figure 4.4 and Figure 4.5 show the traveltime shifts calculated for the fast and slow polarizations of the converted-wave seismic, respectively. The western half of Wishbone shows more traveltime change. Differences in traveltime across the section appear to be divided more north to south across the east-west trending graben than east to west, as phase shifts were seen to vary.

Traveltime shifts in the PS1 data show that the monitor seismic data were slower near stimulated areas of the reservoir. Positive shifts are observed only near faults near the edges of the survey and are of suspect accuracy. The largest magnitude shifts are west of Wishbone section along the large fault set striking NE-SW. The shifts blend and extend eastward across the northern half of Wishbone section and diminish in the east. The shifts truncate along the E-W trending graben that cuts Wishbone. In the west, shifts extend southward through Wishbone and continue south following fault geometries to the boundaries of the survey.

In the slow converted-wave data, traveltime shifts are less clear but show the largest magnitude west of Wishbone, in Wishbone, and east of Wishbone. Shifts do not cover as great an extent as in the fast polarization and follow faults but less distinctly than in the PS1 data. The difference in magnitude of shifts between the polarizations again suggests that the PS1 encounters more change in the reservoir between baseline and monitor. Again, this could be related to how these data were rotated during processing or medium symmetry.

Traveltime shifts in the PS data provide a dimension of information not available in the PP data. Yet, they highlight similar areas of the survey and show less response around the edges of the survey.

4.4 Shear-wave phase shifts

Phase shifts calculated in the shear data have the largest magnitude of any mode of data, ranging between −30 and 30 degrees. The phase response of both polarizations appears similar (Figure 4.6 and Figure 4.7), but shifts are larger and more extensive for the fast mode. Larger phase shifts exist in the western half of Wishbone with the largest phase shifts lying outside of Wishbone to the west. A lesser, though notable, response is seen outside of Wishbone to the east as well. The response of both modes corresponds to the location of some surrounding wells, but a response was not measured around all wells outside of Wishbone. As in the converted-mode data, the results from these polarized data reveal an anisotropic effect, and faults impact the distribution of shifts.

The S1S1 data show the largest magnitude phase shifts of any of the data. These large shifts lie west of Wishbone under the wells stimulated during monitor acquisition. Here, the distribution of shifts appears to follow the well geometry more than fault geometry. To the east, phase shifts extend from this region following faults to the south and north. In Wishbone, shifts are localized in the northwestern quadrant of the section and truncate against faults. Shifts appear east of Wishbone, too.

More extensive, though lesser magnitude shifts appear in the S2S2 data than in the S1S1 data. The largest shifts for this polarization, however, occur to the west of Wishbone. Shifts appear around faults to the south of Wishbone, and more shifts occur in Wishbone below the E-W trending graben than in the S1S1 data. Shifts track eastward along the graben to another area of shifts below the well east of Wishbone. In Wishbone particularly, the presence of shifts appears to be related to well spacing. More, larger magnitude shifts occur around closely spaced wells, while few shifts, save those around the graben, appear around the two easternmost Wishbone wells.

4.5 Shear-wave traveltime shifts

Similar to maps generated for the converted-wave data, traveltime shifts are larger and more widespread for the fast polarization of the shear wave than the slow polarization (Figure 4.8 and Figure 4.9). Calculated traveltime shifts in the shear mode gave the largest magnitude, up to about 6 ms, of traveltime shifts calculated in any of the data. Shifts are limited to the area west of Wishbone and correspond to the areas showing the largest phase response. Most of the traveltime shifts appear around the southwest-northeast trending fault that intersects the western half of Wishbone, and traveltime shifts are distributed differently than the phase shift measurements for both polarizations. Again, faults bound time-shift measurements.

The S2S2 data show almost no traveltime shifts. Although the S1S1 data show more shifts, the shear-wave data as a whole show less traveltime change than the converted-wave data. Shifts in the shear data are of larger magnitude even if they are of lesser extent. As in each of the other data, the largest shifts are west of Wishbone and in the west of Wishbone. The eastern Wishbone wells show no traveltime shifts in either polarization of the shear-wave data.

The larger response in the S1S1 suggests that the fast polarization experiences more change than the slow polarization, and in both polarizations, show almost exclusively negative traveltime shifts. Like the PS data, the SS traveltime-shift maps indicate an anisotropic response in the reservoir, and, consistent with all of the other seismic data, show the most phase response in the western portion of the survey.

4.6 Results summary and maps

The maps below provide five primary observations that will be considered during interpretation.

- Each mode of data shows a different shift response. Traveltime and phase shifts increase through the compressional-, converted-, and shear-mode data. The converted- and

shear-mode data show more widespread shifts than the compressional-mode data as well.

- The converted- and shear-mode shift maps reveal an anisotropic response, showing that the fast and slow polarizations are perturbed differently by the subsurface.
- The western half of Wishbone shows a stronger phase-shift response than the eastern half of Wishbone section.
- Phase shifts appear outside of Wishbone section and correlate to the locations of some wells that surround the section.
- Fault geometry influences phase shift distribution in each mode.

From these observations I hypothesize that where phase and traveltime shifts are measured, the subsurface has been changed between baseline and monitor acquisition. Modeling suggested that phase shifts could be due to interference or attenuation differences between baseline and monitor seismic, and traveltime shifts could be due to velocity variations caused by changing reservoir conditions. During interpretation, external data are incorporated to investigate whether actual changes in the subsurface correlate to calculated shifts and how these might affect the seismic wavefield.

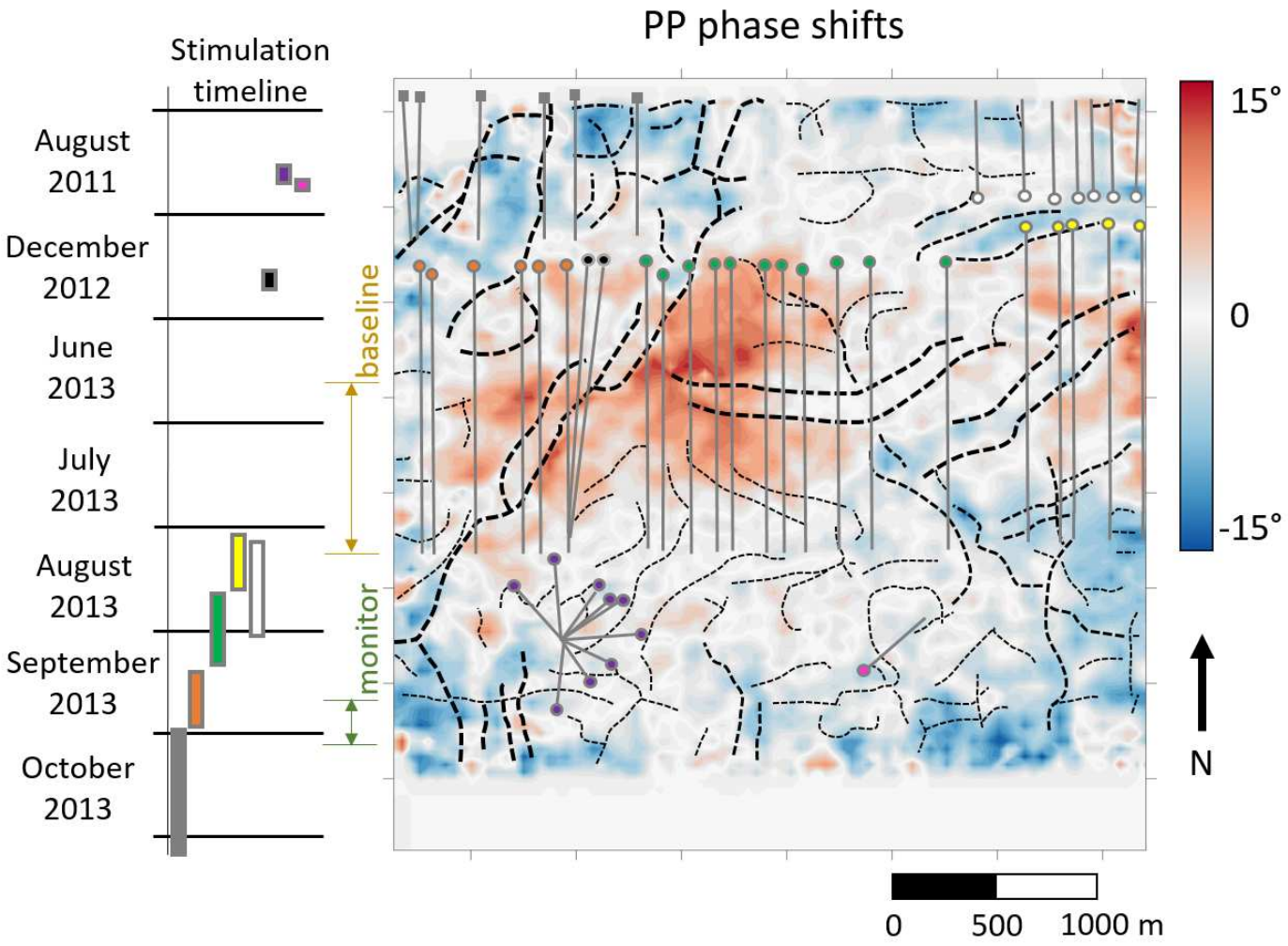

Figure 4.1: Phase-shift map for the compressional-wave data at the base reservoir reflection.

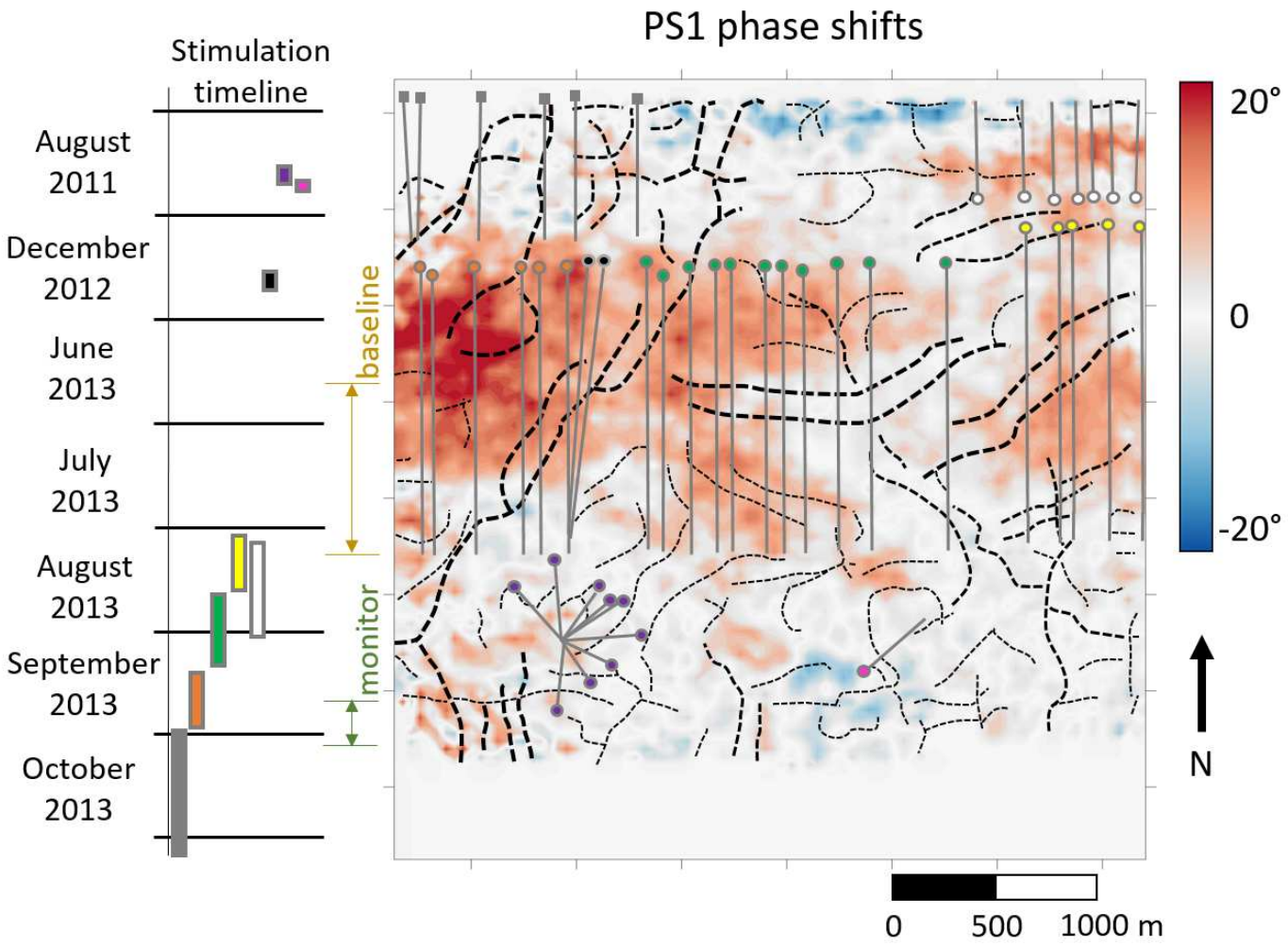

Figure 4.2: Phase-shift map for the fast converted-wave data at a reflection near the reservoir base.

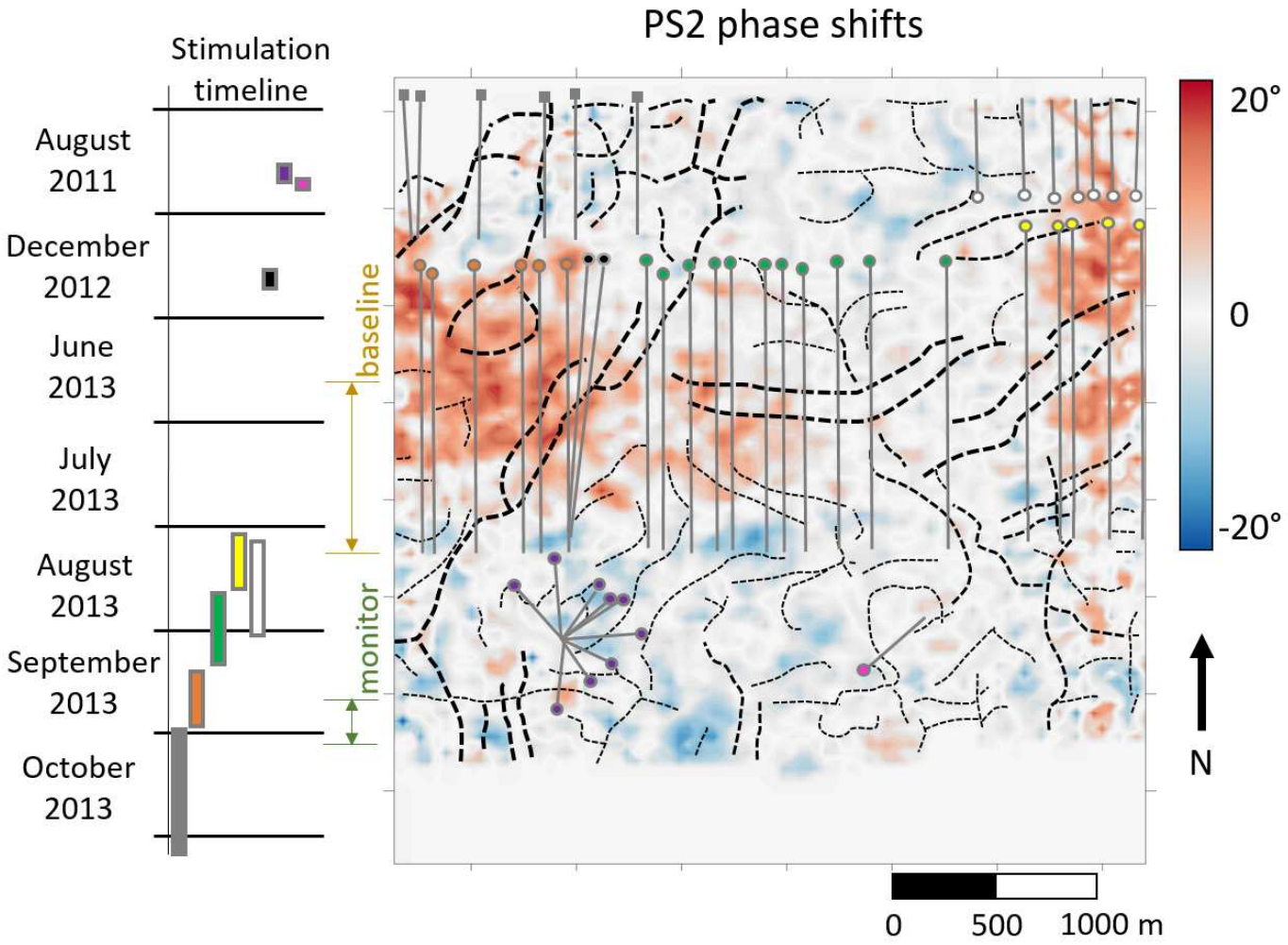

Figure 4.3: Phase-shift map for the slow converted-wave data for a reflection near the reservoir base.

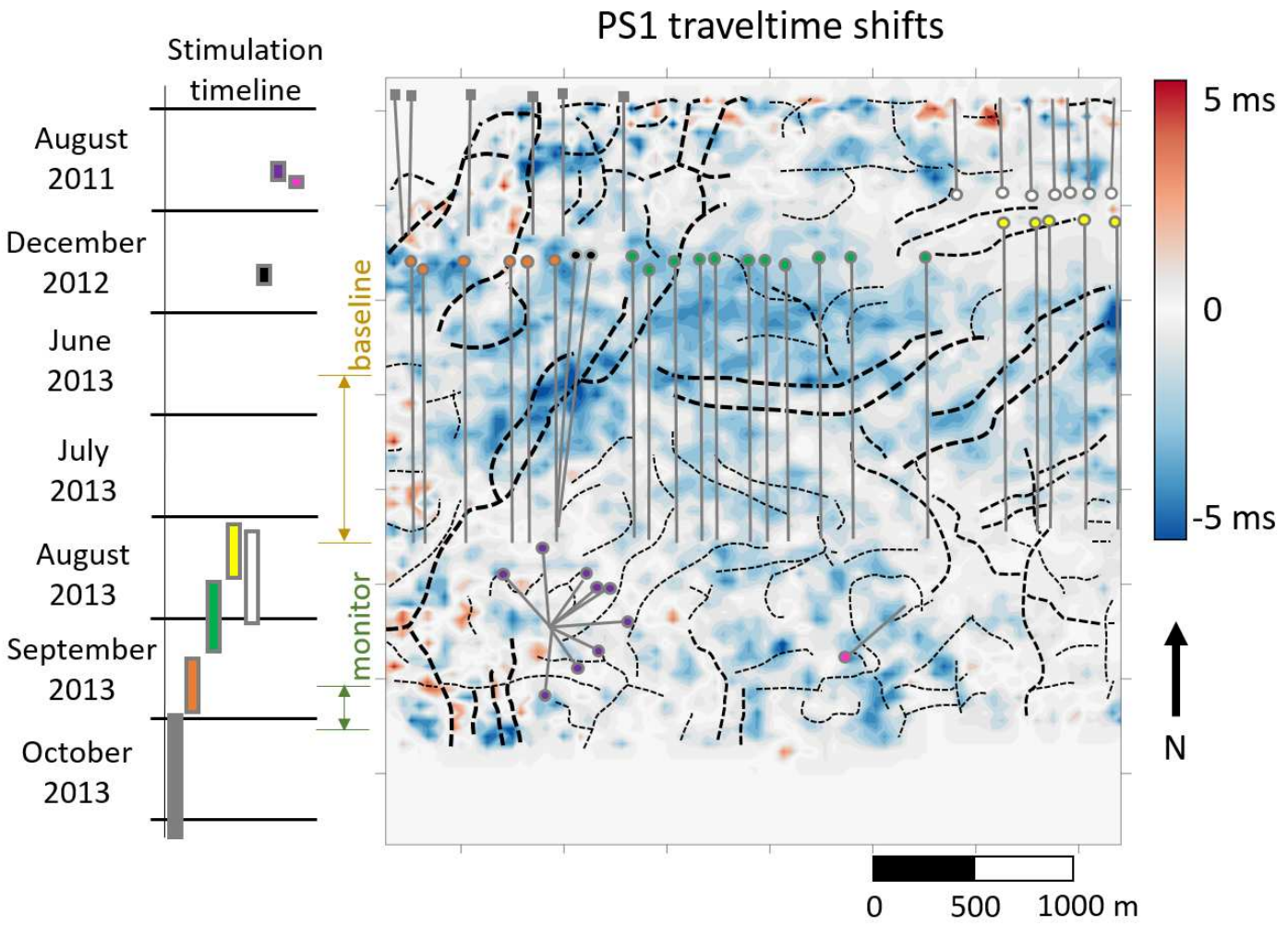

Figure 4.4: Traveltime-shift map for the fast converted-wave data at a reflection near the reservoir base.

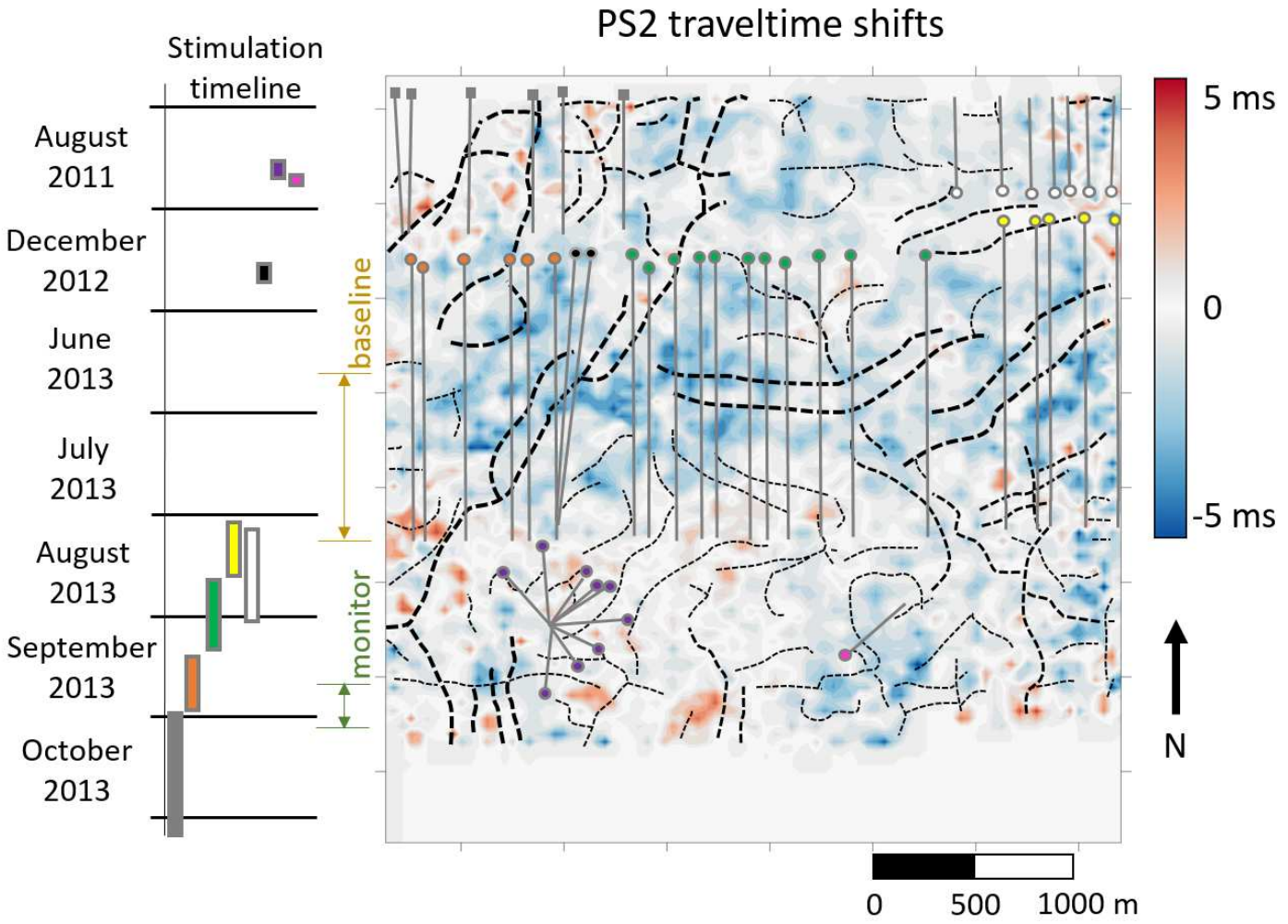

Figure 4.5: Traveltime-shift map for the slow converted-wave data at a reflection near the reservoir base.

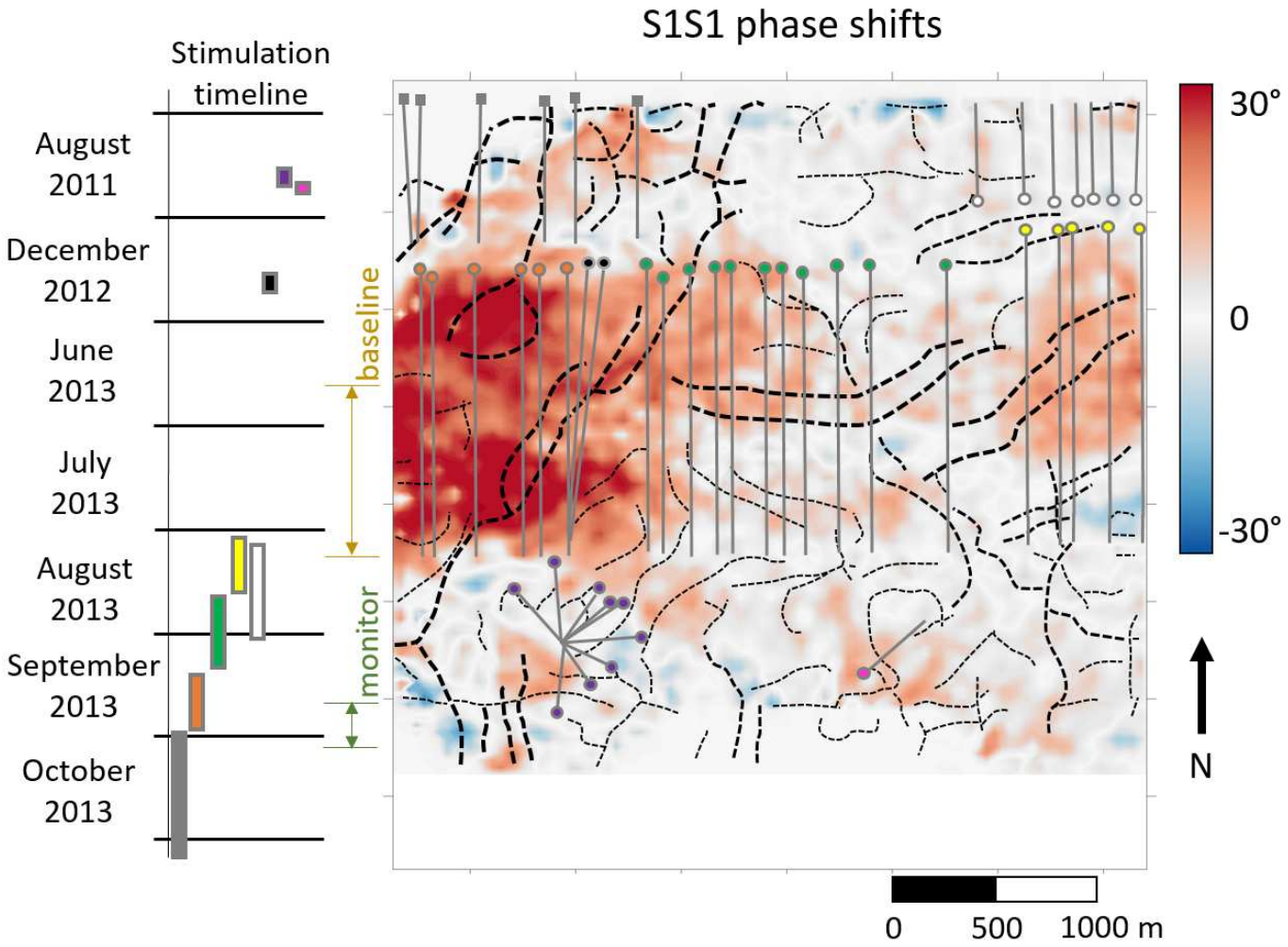

Figure 4.6: Phase-shift map for the fast shear-wave data at a reflection near the reservoir base.

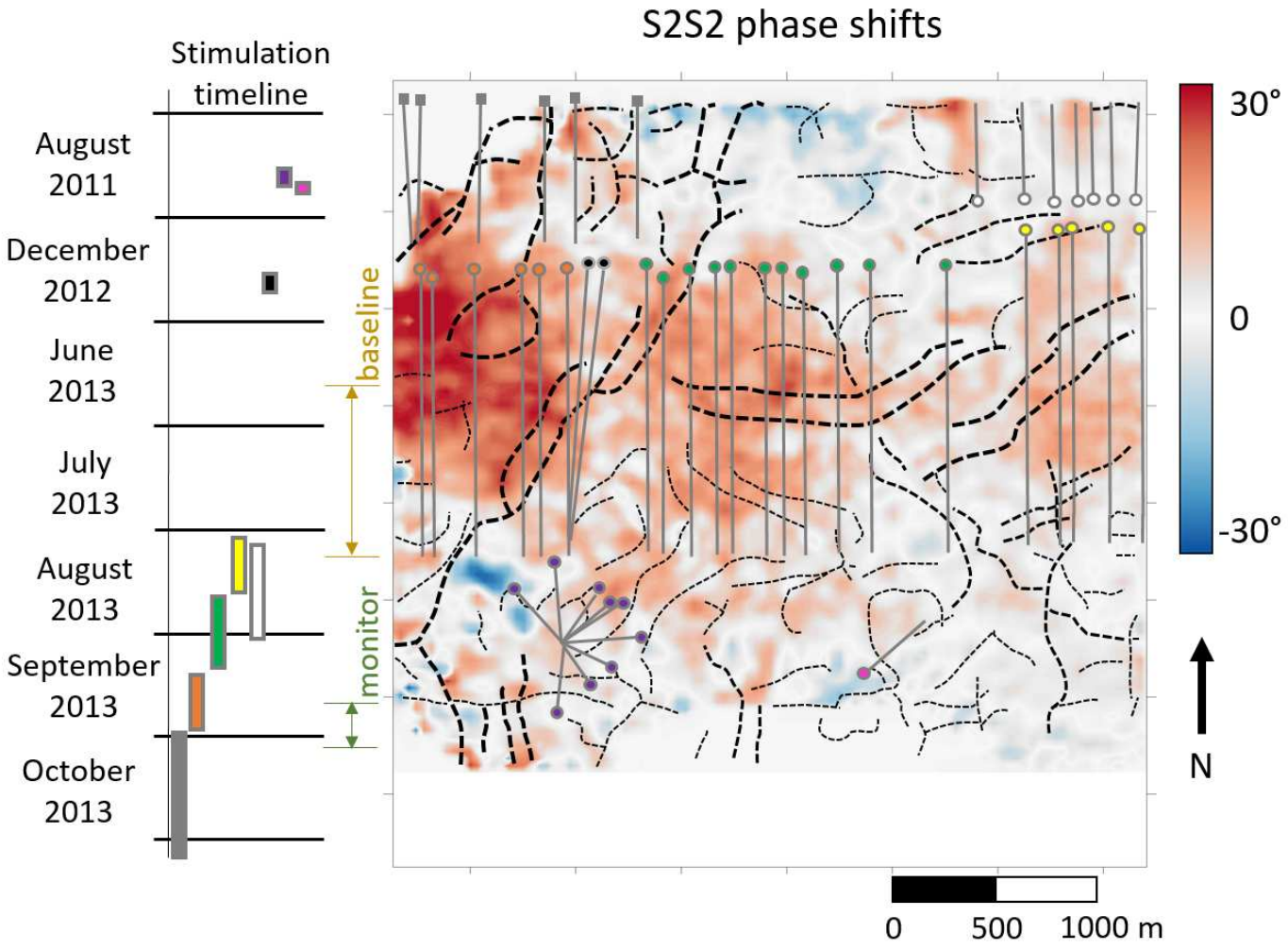

Figure 4.7: Phase-shift map for the slow shear-wave data at a reflection near the reservoir base.

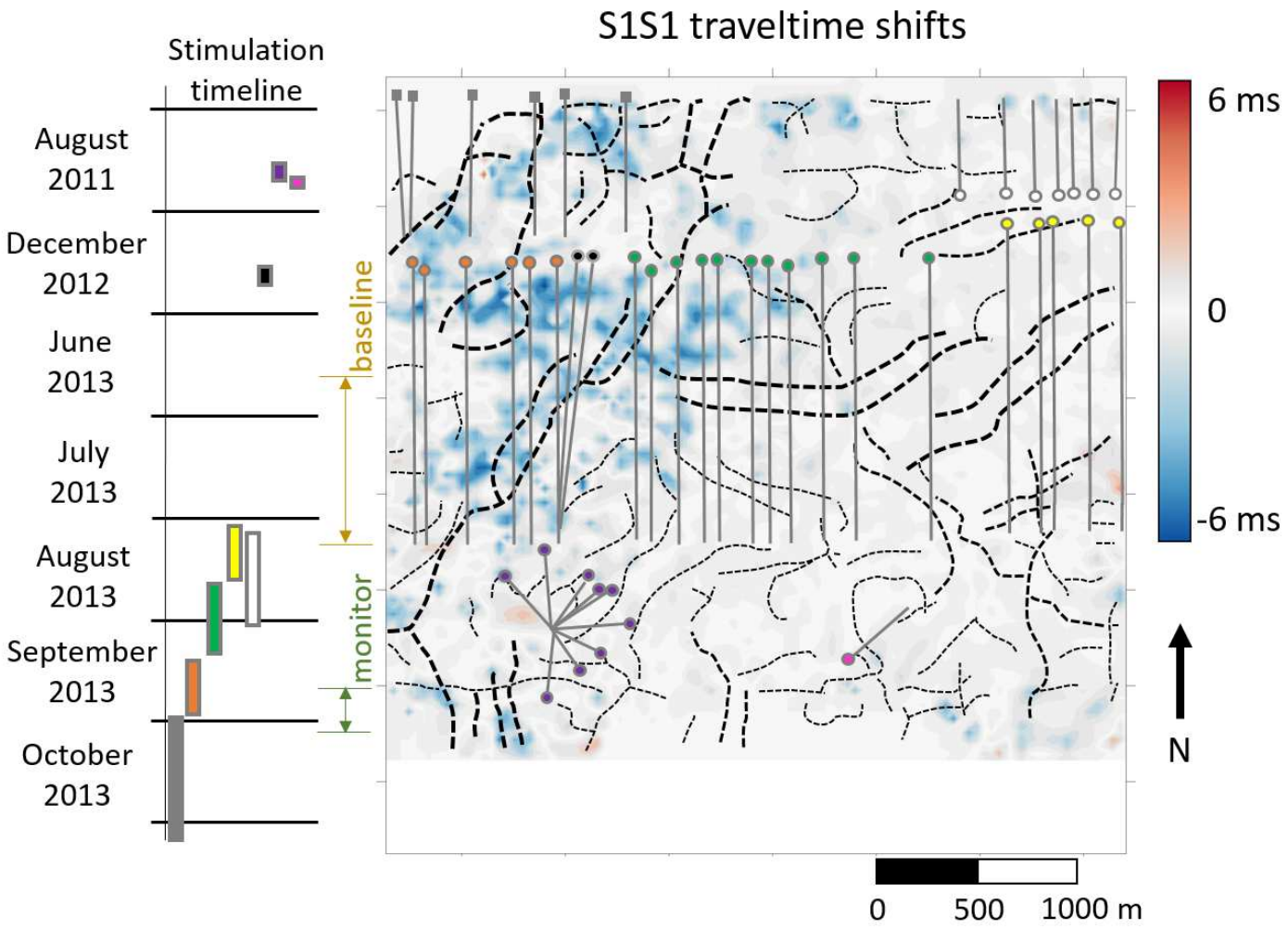

Figure 4.8: Traveltime-shift map for the fast shear-wave data at a reflection near the base reservoir.

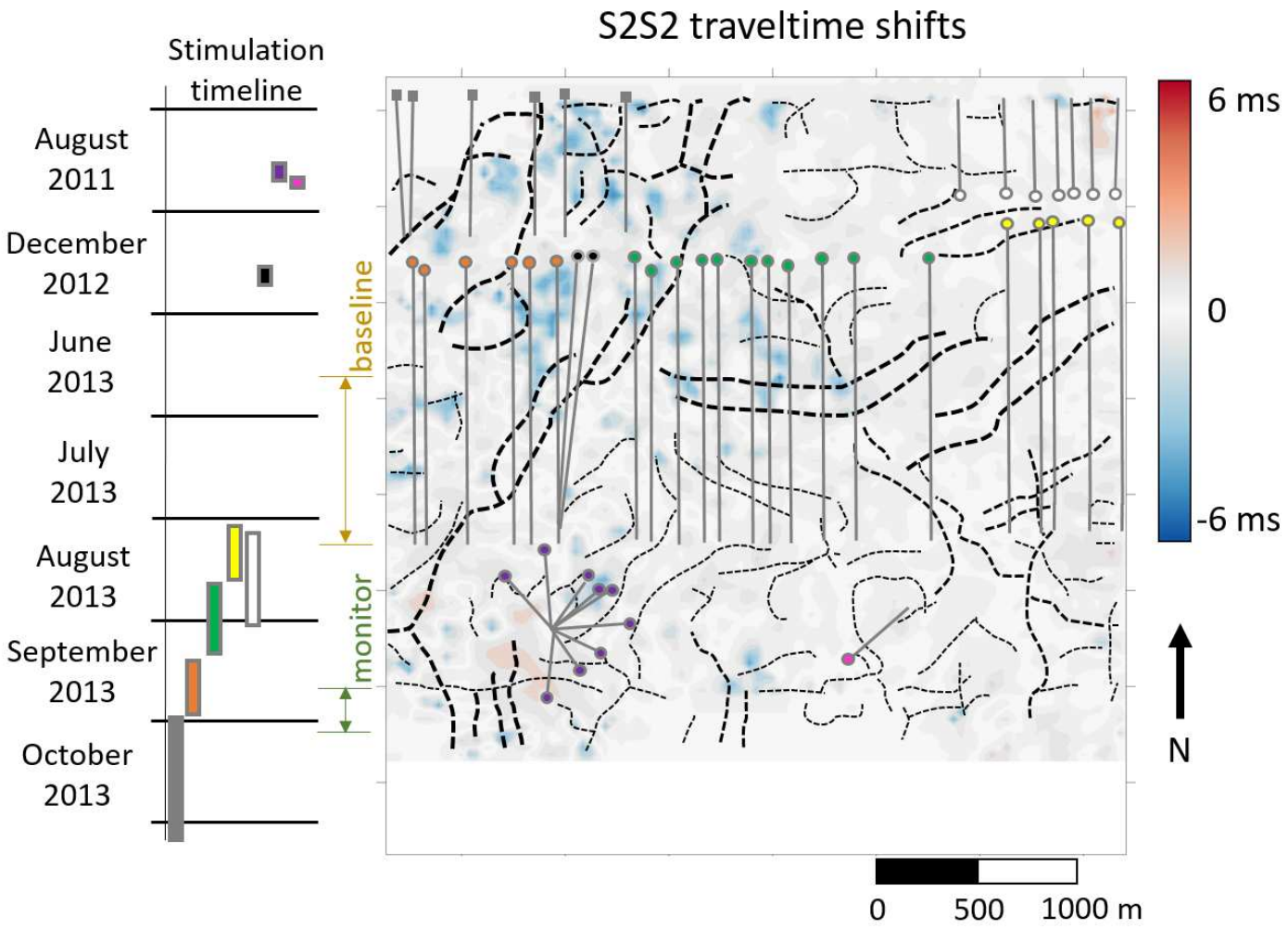

Figure 4.9: Traveltime-shift map for the slow shear-wave data at a reflection near the base reservoir.

CHAPTER 5

INTERPRETATION

Recalling observations made from the traveltime- and phase-shift maps, interpretation focuses on comparing the eastern and western halves of Wishbone section. Figure 5.1 shows the PP phase-shift map with two boxes of equal area drawn. Few phase shifts are seen in the eastern box while many shifts are seen in the western box. External data indicate different physical responses to stimulation occurring in eastern and western Wishbone. Specifically, more fractures are interpreted to be open in western Wishbone during monitor acquisition, and the number of open fractures across the section is proposed to be related to measured phase and traveltime shifts.

Phase results, interpreted as representative of a real change in the reservoir, are corroborated by an independent analysis by White (2015) studying the time-lapse response of acoustic impedance in the reservoir. That study reveals a spatially similar area being perturbed between baseline and monitor surveys as seen in Figure 5.2. That study also shows that between baseline and monitor surveys, acoustic impedance decreased across the reservoir most markedly in the western half of Wishbone, and White (2015) suggests differential pressure across the section to be responsible for the impedance gradient observed.

In Wishbone a correlation between the presence of a phase response and the timing of opening of wells for fluid withdrawal exists. Eastern wells were opened for flowback and production before monitor acquisition had completed, whereas western wells remained shut-in for the duration of the monitor acquisition. Phase response outside of Wishbone correlates similarly to the dates of stimulation of wells surrounding Wishbone. Areas containing wells stimulated before time-lapse seismic acquisition commenced show no phase response, and areas containing wells stimulated after monitor acquisition had completed show no phase response. Areas around wells stimulated between baseline and monitor acquisition periods

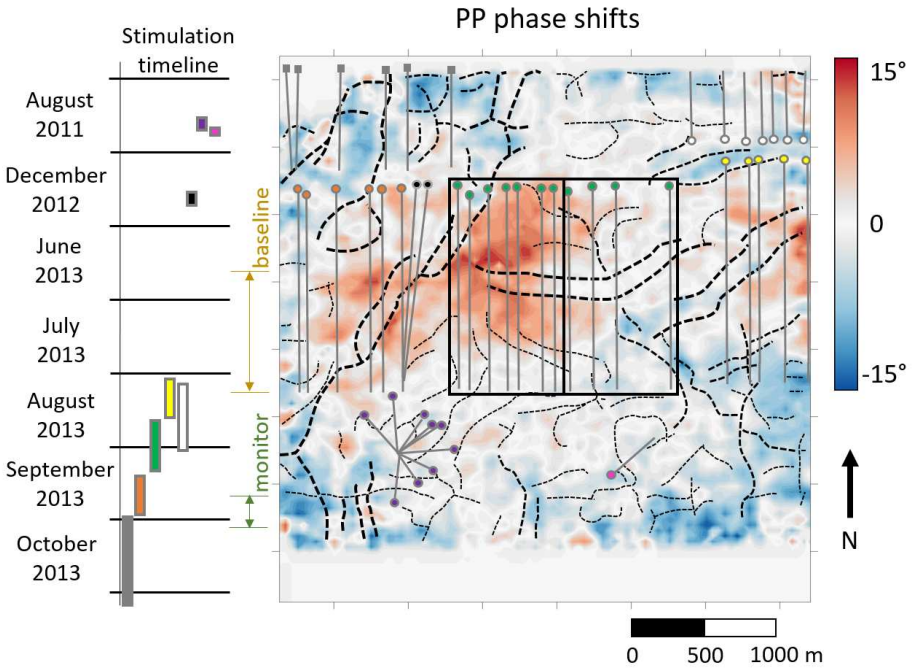

Figure 5.1: Phase-shift map for the compressional data with Wishbone divided into eastern and western subsections of equal area.

and those stimulated during the monitor acquisition period show the largest phase responses. The correlation of well stimulation date across the entire survey area to phase response is 1:1, suggesting that as wells are opened for fluid withdrawal, phase response diminishes.

Two primary variables changing in the reservoir as fluid is withdrawn are reservoir pressure and fracture aperture. Both fracture aperture and reservoir pressure are greater when a larger volume of fluid fills the reservoir, and both are at a maximum when wells are being stimulated and when shut-in, since fluid volume is at a maximum during these periods. It would be expected that the wells being stimulated or shut-in during the acquisition of the monitor survey would show the largest phase shifts, and such is observed in these data.

The eastern and western halves of Wishbone have the same area and similar depth and therefore have similar volume. In two equal, fractured volumes of rock, more fractures are opened in the volume in which more fluid is injected. The volume in which more fractures are opened should produce more hydrocarbons, since more reservoir surface area becomes

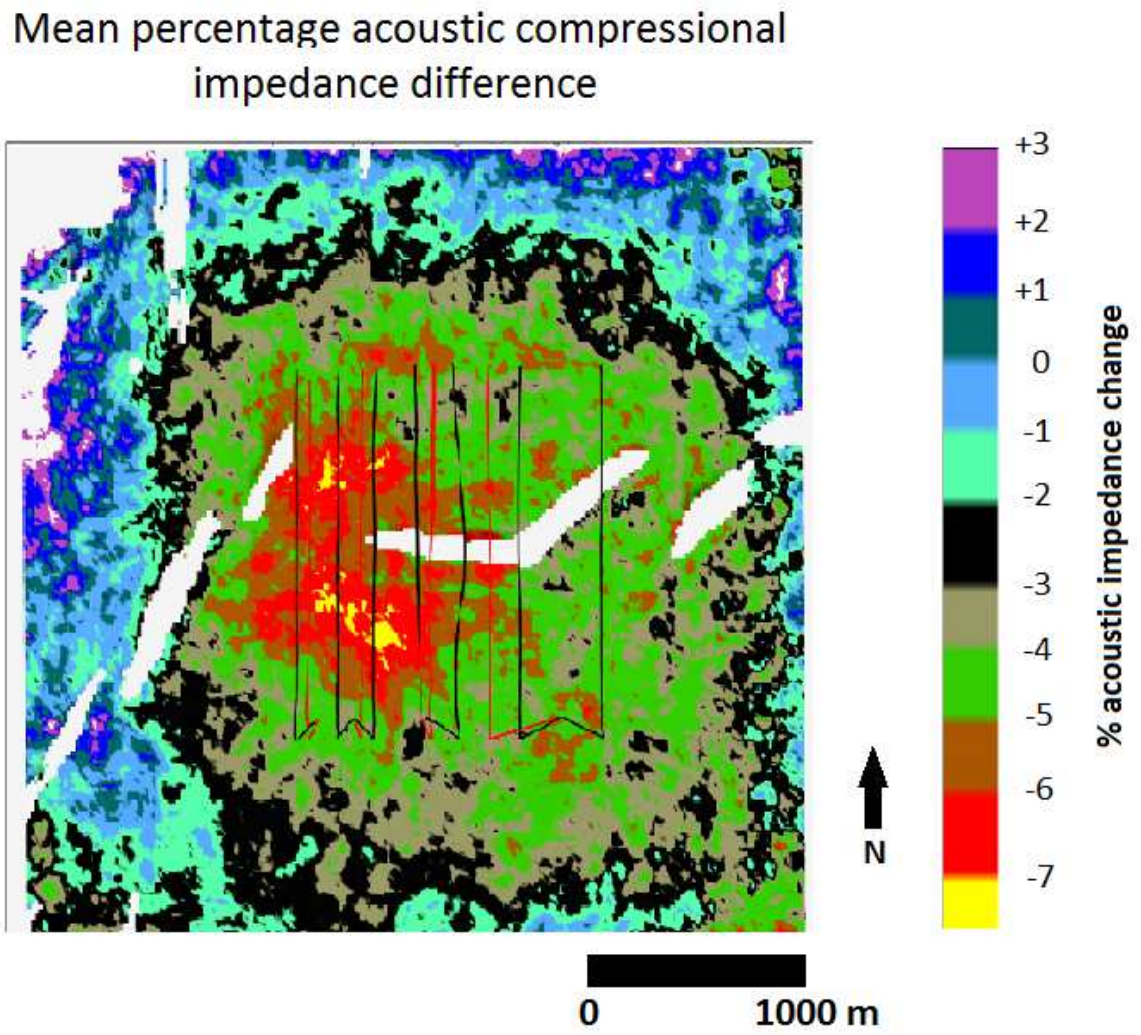

Figure 5.2: Time-lapse percentage acoustic impedance change for the compressional data measured over the reservoir interval. Wells drawn in black are Niobrara wells, and wells drawn in red are Codell wells. (White, 2015).

exposed. Production in Wishbone suggests that greater reservoir surface area is exposed meaning more fractures are opened in western Wishbone.

After two years of production, more fluid was withdrawn from the western half of Wishbone than the eastern half (Figure 5.3). Despite the difference in total volume of fluid withdrawn between east and west, the total extracted fluid volume weighted by the number of wells per subdivision is nearly identical. The total fluid volume withdrawn in the west divided by seven compared to the total fluid volume withdrawn in the east divided by four results in a production difference of less than 1.5%. Similar well efficiency between east and west suggests that the total difference in production between east and west is more related to the number of wells per unit reservoir volume than to lithologic or well completion differences across the reservoir. Even though the Niobrara and Codell make up a regionally heterogeneous reservoir, studies by Dudley (2015) and Matthies (2014) show that local variations in geology are small, and Dudley (2015) shows that fracturing and production are locally independent of lithology. The similarity of production per well compared between east and west also shows that well spacing has not reached a lower limit in the west, suggesting that the east could perhaps sustain additional wells without reducing average per well hydrocarbon production.

Although greater fluid volumes injected in the west suggest more fractures opening in that part of the reservoir, they do not provide a direct observation. Dudley (2015) compares image logs from two wells in Wishbone section, one well located in the eastern half and the other located in the western half. That study shows that the well in the eastern half passed through more faults and fractures yet produced less than the well located in the western half of Wishbone (Dudley, 2015). After two years of production, the western well remains a better producer. Dudley (2015) notes, however, that the eastern well contained fewer fracture stages than the western well and that the eastern well was less clearly connected to a conjugate fracture network despite passing through more natural fractures along the wellpath. Reservoir surface area accessed by a well is a function of whether the well is

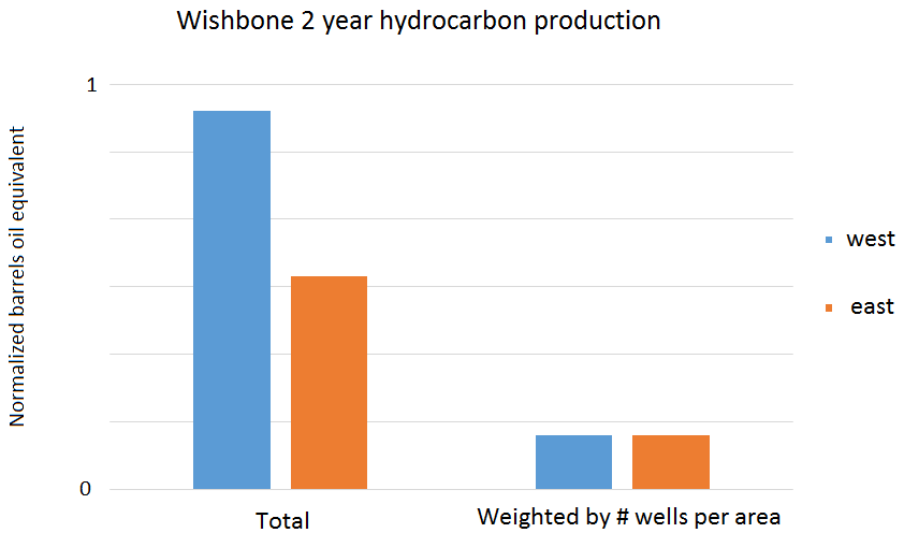

Figure 5.3: Production from eastern and western Wishbone wells over a 2 year period. Total hydrocarbon production and hydrocarbon production weighted per well graphed.

connected to a larger fracture network and the extent of the fracture network.

Tracer analysis by Dang (2015) suggests that wells across Wishbone section are all connected hydraulically, possibly indicating that all of the Wishbone wells are part of a large fracture network that extends throughout the reservoir including the Niobrara and Codell units. Connection to the same fracture network could explain the similar average hydrocarbon production across the reservoir, which indicates similar average volumes of the reservoir being drained per well. Yet since more wells lie in the west, a greater total reservoir volume is drained, as shown by the total production. More total volume drained indicates more fractures opened. Opening a fracture means increasing the volume of the fracture by increasing its aperture. Fractures within highly stressed rock tend to close unless they are held open by a force that counteracts the tectonic stresses pressing the rock. Injecting highly pressured fluid with proppant does exactly this and is the purpose of hydraulic stimulation. To create a more voluminous fracture, more fluid (and/or proppant, natural or synthetic) must be injected.

A significantly greater volume of fluid was injected into the western half of Wishbone than into the eastern half. As mentioned, unless much of the injected fluid was lost, more fractures, including fractures within natural fracture networks, must be opened in the west. More open fractures result in more reservoir surface area accessed, and production data shows more hydrocarbon production, which is related to reservoir surface area, in the west of Wishbone. In addition, since more fluid was injected in the west, higher reservoir pressure should result, and Dang (2015) shows a pressure gradient across the section with higher pressure in the western half of Wishbone than in the east. Uneven pressurization across the reservoir results in different fracture apertures across the reservoir, and phase shifts seen following faults may indicate that faults provide paths for migration for pressure and fluids in the reservoir. Faults can also be barriers, since although Wishbone wells are all connected to a shared fracture network, phase shifts do not extend into eastern Wishbone but cease along the NW-SE fault that cuts through the section. Compartmentalization keeps the reservoir from being pressured uniformly.

Microseismic provides a good standard against which to scrutinize the interpretation of more fractures being opened in western Wishbone than the east, since microseismic events are good indicators of the opening of new fractures or the opening of existing fractures in reservoirs. Microseismic analysis performed by Quezada and Duncan (2015) shows the same as suggested by other data, that more fractures were opened in the western half of Wishbone section during stimulation. Figure 5.4 from Quezada and Duncan (2015) published in an Hart Energy trade journal article shows microseismic event density plotted in a cross section cutting the 11 Wishbone wells, and the western half of Wishbone indicates higher event densities with greater density between closely spaced wells.

Finally, traveltime-shift maps for the converted- and shear-mode seismic indicate reservoir changes in the western half of the survey and around the toe of wells, similar to the distribution of phase shifts particularly in the converted-wave data. Traveltime shifts in general can be attributed to compaction or velocity changes in the subsurface. Here they

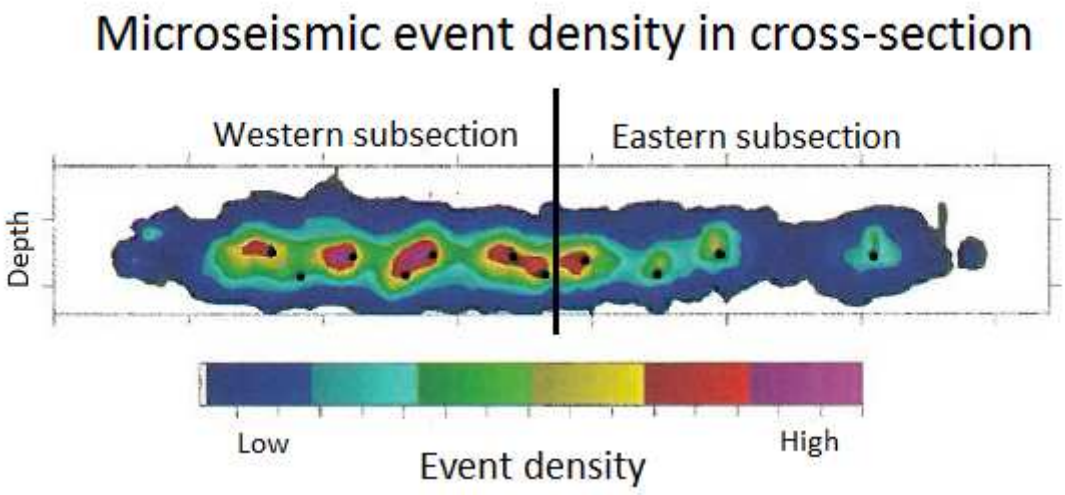

Figure 5.4: Cross section of Wishbone section showing microseismic event density with wells. Warmer colors indicate greater density of microseismic events recorded during stimulation of the wells. (Quezada and Duncan, 2015)

are attributed solely to velocity changes, since the reservoir is fully mechanically compacted (Sonnenberg, 2013).

Changes in pressure can cause seismic velocity to vary, and the traveltime response of each mode is different, especially the converted and shear modes from the compressional mode. Within the converted- and shear-mode seismic, the response of the fast and slow polarization differs, indicating an anisotropic response. In anisotropic material the effect of pressure does not vary with direction, and pressurization might be expected to have the same effect in both polarizations. The anisotropic response may then suggest that reservoir pressurization alone is not responsible for traveltime shifts. Rather, the anisotropic traveltime-shift response may indicate fractured media to which converted- and shear-wave seismic are more sensitive than compressional seismic. If traveltime shifts indicate fractured media, the change in traveltime between baseline and monitor for the converted and shear modes is possibly a response to fractures opened during stimulation.

From all considered data, it is reasonable to interpret that more open fractures were present in the western half of Wishbone than in the eastern half during monitor seismic

acquisition. No data contradict this interpretation, and phase shifts correlate to areas interpreted to contain more open fractures. The data suggest a relationship between open fractures and phase-shift measurements, which has also been suggested in some other studies.

5.1 Fractures and phase

Burns et al. (2007); Fang et al. (2013b); Willis et al. (2006) investigate phase measurements as indicators of fracturing in reservoirs, though not in a time-lapse sense, with wavelet based methodologies. Seismic traces are complex aggregates of interfering reflected and scattered signals from subsurface formation interfaces and heterogeneities, including fractures (Burns et al., 2007). Fracture properties such as stiffness and geometry affect seismic waves traveling through rock, and Willis et al. (2006) show that fractures can scatter seismic energy. Scattered seismic energy from fractures interferes with coherent propagating seismic energy and as a result changes the phase of seismic energy traveling through fractured media. Interference can also potentially cause attenuation, which alters phase as well. In fact, the phase response is azimuthally dependent as Burns et al. (2007) shows that seismic data acquired normal to fracture strike display scattered energy that is canceled during the stacking process. Data acquired parallel to fracture strike contain scattered seismic energy that is enhanced by stacking, which perturbs the seismic wavefield (see Figure 5.5).

These observations are significant because in this research, phase shifts for the converted- and shear-mode seismic show an azimuthally anisotropic response. Based on the work of Burns et al. (2007); Fang et al. (2013b); Willis et al. (2006), such an effect could be related to fracture geometry. Any azimuthal response here may be altered or subdued, however, since the data considered herein are stacked for all azimuths. Nonetheless, in the converted seismic, the fast polarization shows a much stronger phase response than the slow polarization. The difference in response between polarizations conceivably indicates something about fracture orientation. The fast polarization has been interpreted to be oriented parallel to dominant fracture strike (N70W) and maximum horizontal stress, but my results suggest complex

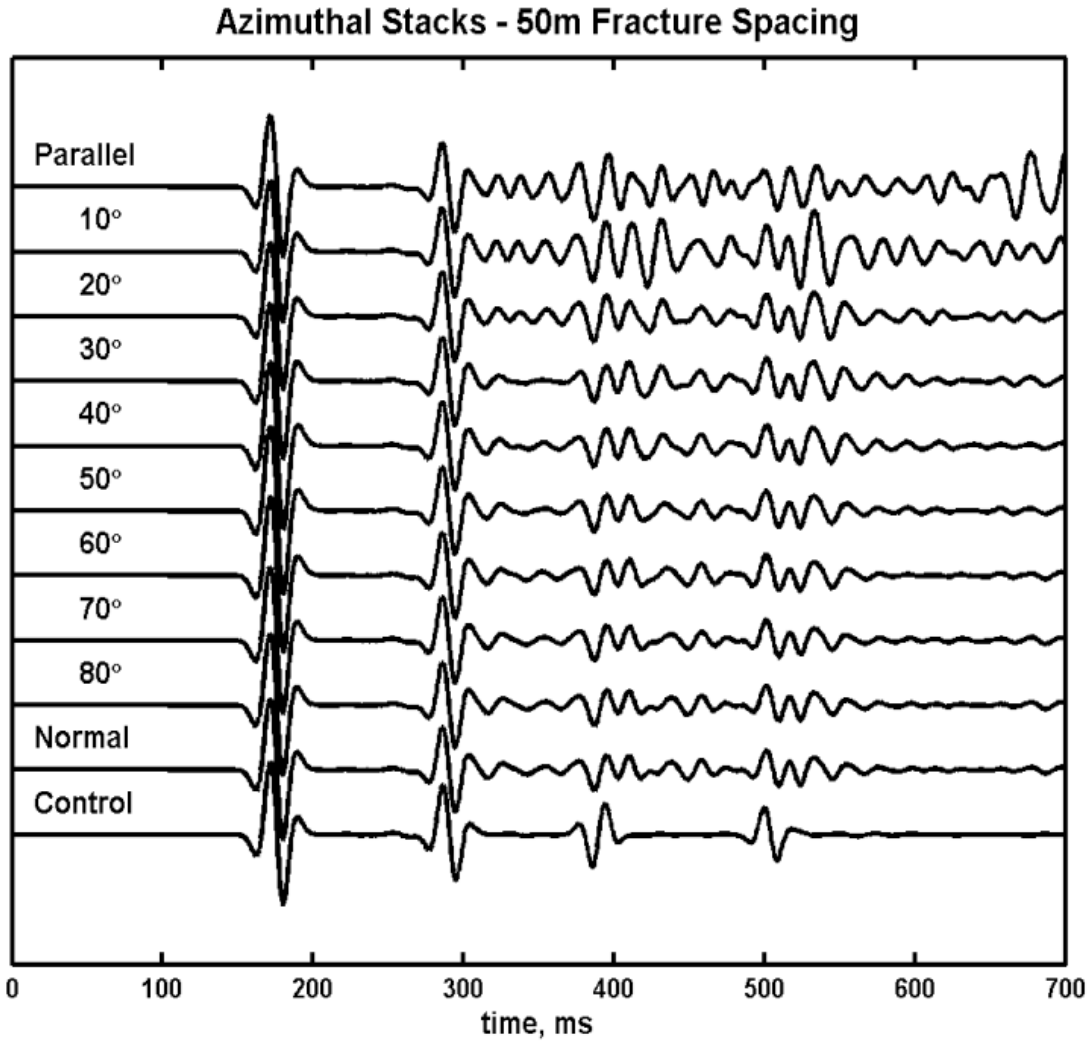

Figure 5.5: Azimuthal dependence of phase perturbations shown by azimuthal stacks of traces from phase modeling performed by Burns et al. (2007). The bottom control trace shows the stack for the model with no fractures. The largest perturbation is seen in the trace parallel to fracture strike while the least response is seen on the trace normal to fracture strike. Figure from Burns et al. (2007).

fracture geometries. Since the fast polarizations show more phase response, fractures might be expected to open parallel to this polarization. If this were the case, then the largest traveltime shifts should be observed in the slow polarization, since seismic energy in this polarization would travel perpendicular to fractures. Like the phase shifts, though, the largest traveltime shifts occur in the fast polarization. This suggests that fractures do not open along a single orientation but in multiple directions and that fracture geometry is complex and irregular, which in turn causes a complex seismic response. There may be multiple fracture sets with various orientations opened. This is highlighted in the shear-mode data, in which a strong phase response occurs in both polarizations of the data suggesting open fractures in multiple orientations.

In addition to a difference in response of the polarizations within the modes of data, a difference in the magnitude of phase response of each mode was observed as well. Recalling the results of the modeling chapter and although the relationship of the trends resulting from the thin layer test were unclear based on the extent of the modeling, they showed that phase-shift magnitude increased with increasing reflectivity of the inserted layer. This may explain the difference in response of the different modes of seismic data. Open, fluid-filled fractures have different reflectivity characteristics relative to the mode of the seismic energy impinging on the fracture. The particle motion of different modes occurs in different directions during propagation, and when these modal waves encounter the same fracture, they experience different stiffness properties of the fracture, which can be related to fracture aperture. This results in different reflectivity characteristics for each mode when propagating though the same rock volume. Additionally, the modes interact differently with fluids, which are ubiquitous in the subsurface. Compressional waves propagate in fluids while shear waves do not. This causes compressional and shear waves to reflect differently when they encounter fluid-filled fractures.

Fracture size relative to seismic wavelength is an important factor in how fractures scatter seismic energy (Fang et al., 2013a). Each mode of seismic considered here has different

wavelength. Thus, each mode likely illuminates fractures of different size or is more or less affected by scattering based the dominant frequency of the seismic energy and the predominant fracture size. Either could cause the different magnitudes of phase response between the modes. These multicomponent data possibly indicate complexly fractured media composed of fractures with various orientation and size.

5.2 Interpretation summary

The western and eastern halves of Wishbone show different phase responses, and each seismic mode provides a unique response. A variety of data reasonably suggest that more fractures were opened in the western half of Wishbone during stimulation, which correlates to observed phase shifts. Phase shifts further correlate to areas outside of Wishbone where other wells have been stimulated, particularly around wells stimulated during acquisition of the monitor seismic survey where more open fractures are expected.

Several studies have shown that fractures scatter seismic energy, which can cause interference and attenuation in recorded seismic signals. From modeling, both interference and attenuation are reasonable, interdependent mechanisms that can cause phase shifts, and phase shifts in these time-lapse data may show wavefield perturbations caused by interference and attenuation from seismic energy scattered by fractures opened in the reservoir during stimulation. The amount of interference, and therefore magnitude of phase shift, is related to reflectivity and fracture size and orientation. Size, orientation, and aperture may be the reason for the different phase response between modes of data, in which the converted and shear mode provide the clearest phase result and are interpreted to reveal the most information about the reservoir. The converted- and shear-mode response may be closely related to fracture characteristics in the reservoir while the compressional-mode response is distinct and possibly indicates compartmentalization, controlled by faults, of areas of relatively higher reservoir pressurization. The converted- and shear-mode data suggest complex fracture geometry.

Phase shifts have been interpreted to reveal areas where fractures have been opened and may also indicate areas where fractures have closed as wells were opened for flowback and production, that is, eastern Wishbone. A measured reduction in phase-shift magnitude and extent from any later monitoring seismic acquisition might show where fractures have closed, where fractures were not effectively propped. Fluid data show that well spacing has not reached a minimum in the section, and large magnitude phase shifts, which are interpreted to indicate open fracture density, correlate to fault intersections and fault tips, which are suggested as drilling targets during later field development. Converted and shear modes appear to provide the most information about the stimulated reservoir, and prestack analysis of phase shifts might provide fracture dimension and orientation information.

Finally, a study of differences in attenuation between baseline and monitor surveys may serve as a useful complement to this study, either confirming or modifying the proposed interpretation. Since scattered seismic energy may cause attenuation, which is a stress, lithology, and azimuthally dependent characteristic of the reservoir, it may be measured in Wishbone. If any attenuation were measured for these multicomponent data, differences between each mode and polarization would be expected along with differences between the east and west of Wishbone. Any azimuthally varying attenuation might provide information about the rock fabric including fracture orientations and intrinsic anisotropy.

CHAPTER 6

CONCLUSIONS AND RECOMMENDATIONS

From analysis and interpretation of the time-lapse multicomponent data along with external data several reasonable, though not definitive, propositions and conclusions are drawn:

- The difference in phase of waveforms before and after hydraulic stimulation indicates physical changes occurring in the reservoir due to hydraulic stimulation. Phase shifts may be caused by seismic energy scattered by fractures opened during stimulation.
- The western half of Wishbone section is interpreted to contain more open fractures since it shows a stronger phase response, and the western half of Wishbone is more productive than the eastern half.
- All modes of the seismic data revealed phase shifts, and the larger responses in the converted and shear mode compared to the compressional mode are attributed to fracture reflectivity, orientation, and size.
- Compressional phase shifts may indicate reservoir pressurization while converted- and shear-mode phase shifts may indicate more clearly open fractures.

Recommendations from this work include:

- Targeting fault intersections during future simulations to provide access to more open fractures, generating more hydrocarbon production.
- Using phase shifts to help evaluate opportunities for infill drilling where no phase shifts were observed in Wishbone section since well spacing has not reached a lower limit.
- Analyzing phase shifts in prestack seismic, particularly in converted and shear modes, in order to investigate the azimuthal properties of phase shifts. Such an analysis could lend information about fracture dimensions and orientations.

- Performing a study of attenuation in these time-lapse data could provide information related to the anisotropic characteristics of the reservoir as well as the rock fabric, fracture, and stress properties of the reservoir.

REFERENCES CITED

Bishop, T. N. and A. G. Nunns, 1994, Correcting amplitude, time, and phase mis-ties in seismic data: Geophysics, **59**, no. 6, 946–953, doi:10.1190/1.1443654.

Burns, D. R., M. E. Willis, L. Vetri, and M. N. Toksöz, 2007, Fracture properties from seismic scattering: The Leading Edge, **26**, no. 9, 1186–1196, doi:10.1190/1.2780790.

Costain, J. K. and C. Çoruh, 2004, Basic Theory of Exploration Seismology: Elsevier.

Dang, A., 2015, Chemical Tracer Study: Fall 2015 Meeting Report, Colorado School of Mines Reservoir Characterization Project, 74–81.

Dudley, C., 2015, Integrating horizontal borehole imagery and cluster analysis with microseismic data for Niobrara/Codell reservoir characterization, Wattenberg Field, Colorado, USA: M.S. thesis, Colorado School of Mines.

Fang, X., M. Fehler, T. Chen, D. Burns, and Z. Zhu, 2013a, Sensitivity analysis of fracture scattering: Geophysics, **78**, no. 1, T1–T10, doi:10.1190/geo2011-0521.1.

Fang, X., M. Fehler, Z. Zhu, Y. Zheng, and D. Burns, 2013b, Reservoir fracture characterization from seismic scattered waves: Geophysical Journal International, doi:10.1093/gji/ggt381.

Huang, N. E., Z. Shen, S. R. Long, M. C. Wu, H. H. Shih, Q. Zheng, N.-C. Yen, C. C. Tung, and H. H. Liu, 1998, The empirical mode decomposition and the Hilbert spectrum for nonlinear and non-stationary time series analysis: The Royal Society, **454**, no. 1971, 903–995, doi:10.1098/rspa.1998.0193.

Lee, W. H. K., H. Kanamori, P. C. Jennings, and C. Kisslinger, editors, 2002, International Handbook of Earthquake and Engineering Seismology: Academic Press.

Matthies, N., 2014, Understanding and mapping variability of the Niobrara Formation across Wattenberg Field, Denver Basin: M.S. thesis, Colorado School of Mines.

Pitcher, T. M., 2015, Joint geophysical and geomechanical analysis of in-situ stress, Wattenberg Field, Colorado: M.S. thesis, Colorado School of Mines.

Purves, S., 2014, Phase and the Hilbert transform: The Leading Edge, **33**, no. 10, 1164–1166, doi:10.1190/tle33101164.1.

Quezada, O. A. and P. M. Duncan, 2015, Cracking the Wattenberg Field: http://www.epmag.com/cracking-wattenberg-field-779741, accessed 10 March 2015.

Sheriff, R. E., M. T. Taner, F. Koehler, and D. Frye, 1977, Extraction and interpretation of the complex seismic trace: Indonesian Petroleum Association.

Sonnenberg, S. A., 2013, New reserves in an old field: the Niobrara resource play in the Wattenberg Field, Denver Basin, Colorado: The Mountain Geologist, **50**, no. 4, 143–166.

Taner, M. T., F. Koehler, and R. E. Sheriff, 1979, Complex seismic trace analysis: Geophysics, **44**, no. 6, 1041–1063, doi:10.1190/1.1440994.

White, M. D., 2015, Time-lapse interpretation of P-wave data for a hydraulically fractured reservoir, Wattenberg Field, Colorado: M.S. thesis, Colorado School of Mines.

Willis, M. E., D. R. Burns, R. Rao, B. Minsley, M. N. Toksöz, and L. Vetri, 2006, Spatial orientation and distribution of reservoir fractures from scattered seismic energy: Geophysics, **71**, no. 5, O43–O51, doi:10.1190/1.2235977.